

RESEARCH ARTICLE

Size-reduced embryos reveal a gradient scaling-based mechanism for zebrafish somite formation

Kana Ishimatsu^{1,*}, Tom W. Hiscock¹, Zach M. Collins¹, Dini Wahyu Kartika Sari^{2,3}, Kenny Lischer², David L. Richmond⁴, Yasumasa Bessho², Takaaki Matsui² and Sean G. Megason^{1,*}

ABSTRACT

Little is known about how the sizes of animal tissues are controlled. A prominent example is somite size, which varies widely both within an individual and across species. Despite intense study of the segmentation clock governing the timing of somite generation, how it relates to somite size is poorly understood. Here, we examine somite scaling and find that somite size at specification scales with the length of the presomitic mesoderm (PSM) despite considerable variation in PSM length across developmental stages and in surgically size-reduced embryos. Measurement of clock period, axis elongation speed and clock gene expression patterns demonstrate that existing models fail to explain scaling. We posit a ‘clock and scaled gradient’ model, in which somite boundaries are set by a dynamically scaling signaling gradient across the PSM. Our model not only explains existing data, but also makes a unique prediction that we confirm experimentally – the formation of periodic ‘echoes’ in somite size following perturbation of the size of one somite. Our findings demonstrate that gradient scaling plays a central role in both progression and size control of somitogenesis.

KEY WORDS: Scaling, Somite, PSM, Segmentation clock, Fgf gradient, Quantitative imaging, Mathematical modeling, Zebrafish

INTRODUCTION

Scaling – matching organ size to body size – is a fundamental property of developing organisms. Even within the same species, developing embryos often vary in size, owing to environmental and maternal variability. In addition, embryo size can change drastically across developmental stages. Nevertheless, embryos robustly develop with invariant proportions, suggesting that some mechanism of pattern scaling is encoded in the developmental program (Cooke, 1981). Although the scaling of morphogen-based patterning has received significant attention, both theoretically and experimentally (Ben-Zvi and Barkai, 2010; Gregor et al., 2005, 2008; Inomata et al., 2013; Lander et al., 2011; McHale et al., 2006; O’Connor et al., 2006), understanding has been limited for scaling of other patterning processes. In particular, in the field of somite segmentation, there are currently multiple, mechanistically different models (Cooke and Zeeman, 1976; Cotterell et al., 2015; Lauschke et al., 2013).


During embryogenesis, somites provide the first body segments in vertebrates, eventually giving rise to tissues such as the vertebrae and axial skeletal muscles. Somite segmentation occurs sequentially in an anterior to posterior progression along the presomitic mesoderm (PSM), with temporal and spatial periodicity. Temporal periodicity [e.g. somites are formed in symmetric pairs every 25 min in zebrafish (Schröter et al., 2008)] is known to be generated by a system of coupled cellular oscillators (Delaune et al., 2012; Lauschke et al., 2013; Masamizu et al., 2006; Palmeirim et al., 1997) called the segmentation clock, which is driven and synchronized by complex signaling networks (Dequeant et al., 2006; Hubaud and Pourquie, 2014; Krol et al., 2011). Yet, how these oscillations relate to the spatially periodic pattern of the mature somites and how somite sizes are determined remains controversial (Akiyama et al., 2014; Cooke and Zeeman, 1976; Cotterell et al., 2015; Lauschke et al., 2013; Shih et al., 2015; Soroldoni et al., 2014; Takahashi et al., 2010; Tsiairis and Aulehla, 2016).

Somites were first documented to scale in *Xenopus* following surgical bisection of the egg; the resulting embryos have smaller somites but the same number compared with intact control embryos (Cooke, 1975). Although this experiment was performed more than 40 years ago, the underlying mechanism for somite scaling has not been identified. In particular, the relationship between PSM length and somite size has been disputed: previous groups have reported that in intact developing embryos, somite size does not scale with PSM size (Gomez et al., 2008), whereas in *ex vivo* culture of PSM, somite length has been shown to scale in a linear manner with PSM length (Lauschke et al., 2013).

In this study, using both surgically size-reduced and normally developing zebrafish embryos, in combination with live imaging, quantitative measurement and mathematical modeling, we demonstrate that somite length does indeed scale with PSM length and that gradient scaling underlies somite scaling. We demonstrate that the inconsistency in the reported relationship between PSM size and somite size can be attributed to the time delay between somite specification and morphological boundary formation. We measured this delay experimentally and found that somite length always scales with PSM length when this delay is considered. This result led us to evaluate several variables that could potentially modulate somite length. We found that clock period, axis elongation speed, and clock gene expression patterns did not scale, whereas the Fgf activity gradient did scale with PSM length. Given this observation, we developed a ‘clock and scaled gradient model’ based on the original clock and wavefront model (Cooke and Zeeman, 1976) with a simple yet important refinement: in our model, the gradient responsible for setting wavefront position dynamically scales to the size of the PSM. Using transplants, we show that somite-derived signals can inhibit Fgf signaling, providing a potential mechanism for gradient scaling. The clock and scaled gradient model not only explains existing experimental

¹Department of Systems Biology, Harvard Medical School, Boston, MA 02115, USA. ²Gene Regulation Research, Nara Institute of Science and Technology, Nara 630-0101, Japan. ³Department of Fisheries, Universitas Gadjah Mada, Yogyakarta 55281, Indonesia. ⁴Image and Data Analysis Core, Harvard Medical School, Boston, MA 02115, USA.

*Authors for correspondence (kana_ishimatsu@hms.harvard.edu; megason@hms.harvard.edu)

 K.I., 0000-0002-4434-0088; S.G.M., 0000-0002-9330-2934

data but also inspired a novel experimental test with an unintuitive outcome – the creation of ‘echoes’ in somite size following perturbation of the system. We present the quantitative study of somite scaling as an experimental platform to test the feasibility of multiple theoretical models.

RESULTS

Somite length at specification scales with PSM length throughout developmental time

Although somite length has been shown to scale with overall body length in *Xenopus* (Cooke, 1975), whether somite length scales with PSM size has been controversial (Gomez et al., 2008; Lauschke et al., 2013). To test this relationship, we measured somite length and PSM length using live imaging. Initially, we did not observe a clear relationship between PSM length and somite size (Fig. 1F, without delay). However, somite specification within the PSM occurs long before the appearance of the morphological boundaries (Akiyama et al., 2014; Bajard et al., 2014; Dubrulle et al., 2001; Elsdale et al., 1976; Giudicelli et al., 2007; Ozbudak and Lewis, 2008; Primmitt et al., 1989; Roy et al., 1999) (Fig. 1A), and thus we speculated that the inconsistency with respect to somite scaling could be attributed to this delay. Although previous studies have shown the delay is around four or five cycles, the delay duration could vary at different developmental stages. To examine whether

somite length scales with PSM length when this specification to formation delay is considered, we measured this delay experimentally using embryos from different developmental stages. The dual-specificity phosphatase inhibitor BCI is known to act immediately on Fgf signaling leading to an eventual reduction of somite size (Fig. S1) (Akiyama et al., 2014). We treated embryos transiently at 5 somite stage (ss), 10 ss and 15 ss with BCI and measured the length of the newly formed somites using live imaging for six subsequent cycles (Fig. 1B,C). Regardless of the developmental stage for the pulse BCI treatment, we observed 4-cycle delay on average before a visibly smaller somite formed (Fig. 1D). Our experimentally determined delay is similar, albeit slightly shorter, to what has been proposed in previous work (four or five cycles) (Akiyama et al., 2014; Bajard et al., 2014; Dubrulle et al., 2001; Elsdale et al., 1976; Giudicelli et al., 2007; Ozbudak and Lewis, 2008; Primmitt et al., 1989; Roy et al., 1999). Taking this 4-cycle delay into consideration, we re-examined the relationship between PSM length and somite size (comparing the size of the Nth somite with the PSM size at the N–4 ss, Fig. 1E). Strikingly, we found that somite size does indeed scale with PSM size when this 4-cycle delay is considered (Fig. 1F). No clear relationship between somite and PSM length was apparent without the delay (Fig. 1F). This relationship between PSM length and somite size was still observed with a 3- or 5-cycle delay, suggesting

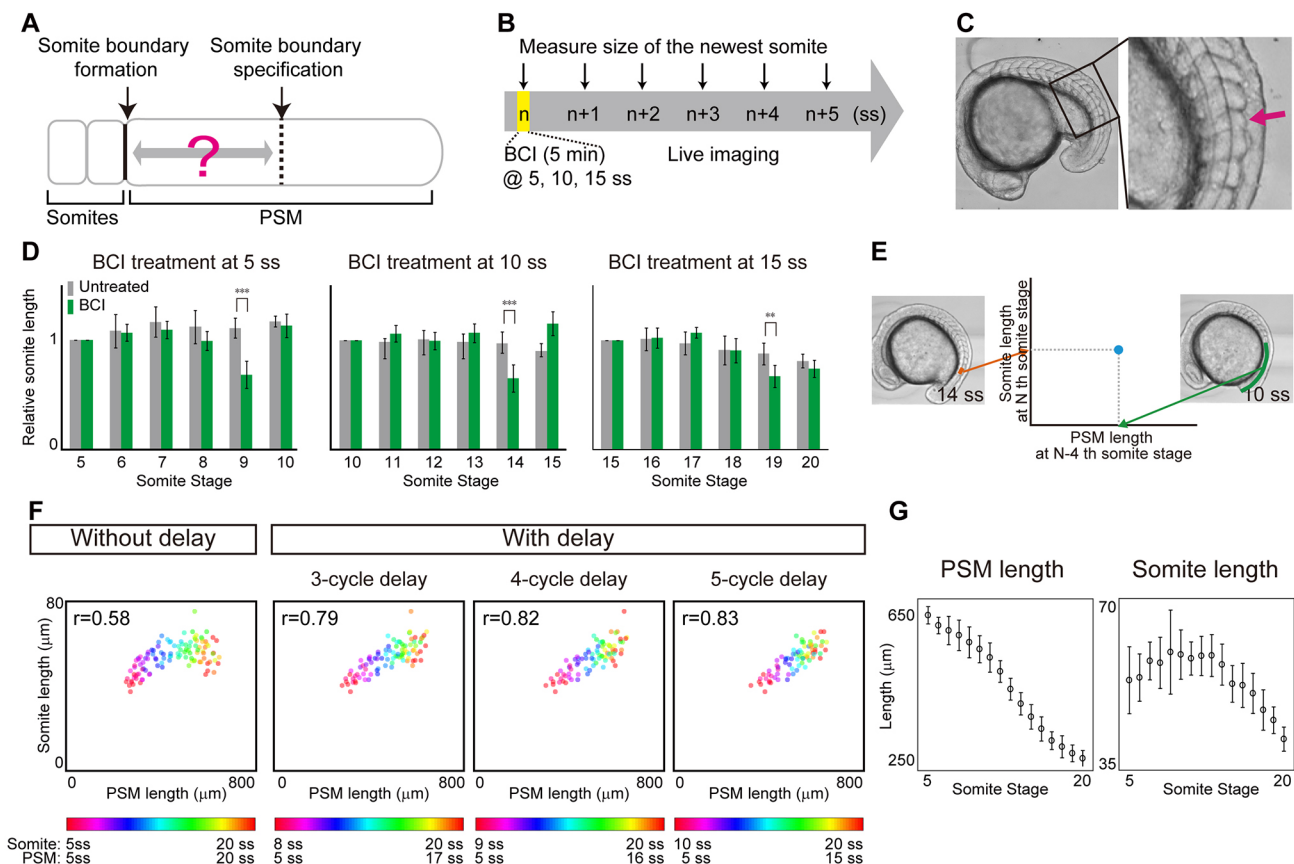


Fig. 1. Somite scaling over time with time delay. (A) Schematic of time delay between somite boundary specification and somite boundary formation. (B) Schematic of the BCI experiment. Embryos were treated with BCI for 5 min and then subjected to live imaging in egg water without BCI. The BCI treatment was carried out at three different somite stages (5, 10, 15 ss), in case the delay time varies over time. (C) BCI-treated embryos form smaller somites (arrow). (D) Relative AP length of somites, normalized by the somite length of control embryos at the somite stage at which BCI treatment was carried out. At each somite stage, the smaller somite was formed four cycles after BCI treatment. Error bars denote s.d. $**P < 0.01$; $***P < 0.001$ ($n=5$ for each condition). (E) Comparison of PSM length and somite length was made using PSM length at N–4 ss (e.g. 10 ss) and somite length at N ss (e.g. 14 ss), using live imaging data. (F) Somite size versus PSM size at different somite stages (indicated by the color scale) with and without time delay of three, four and five cycles ($n=7$). (G) Size dynamics of PSM and somites. Note that the peaks appear at different somite stages. $n=7$ each. Error bars denote s.d.

that minor fluctuations in the delay or measurement error would not affect the conclusion (Fig. 1F). The delay between somite specification and formation is reflected in different peak positions in time course measurements of PSM and somite size (Fig. 1G). Consideration of this delay may be necessary to assess scaling in previous data (Gomez et al., 2008; Schröter et al., 2008).

Somite length at specification scales with PSM length among individuals with different body sizes

Given that somite size at specification scales with PSM length throughout developmental time, we then wondered whether somite length scales with PSM length in zebrafish embryos of varying sizes. Inspired by classic work in *Xenopus* (Cooke, 1975) on somite scaling to body size in surgically size-reduced embryos, we sought to apply this technique to zebrafish. We first attempted to cut zebrafish embryos at the blastula stage longitudinally (along the animal-vegetal axis) as was done in the *Xenopus* study. However, the resulting embryos had varying degrees of dorsalization or

ventralization, presumably owing to dorsal determinants being portioned in unpredictable ways, and were difficult to study quantitatively. We thus developed a method to reduce embryo size without perturbing dorsoventral patterning. By using separate latitudinal cuts to remove cells near the animal pole and yolk near the vegetal pole at the blastula stage (Fig. 2A, left), we found that the resulting size-reduced embryos quickly recovered and a large percentage of them developed normally (Fig. 2A). Total body size and organ size, including somites, of these size-reduced embryos were found to be smaller (Fig. 2B,C). Consistent with previous work in *Xenopus* (Cooke, 1975), the chopped embryos had the same number of somites (33 in both control and chopped embryos at 1 day post-fertilization, $n=5$ for each; somite number was counted using still images of the live embryos), each of which was smaller in size. Combining this size reduction technique and live imaging, we measured somite and PSM length, and found that somite length scales with PSM length between embryos of varying sizes when the same 4-cycle delay is considered (Fig. 2D; see also Fig. S2). The

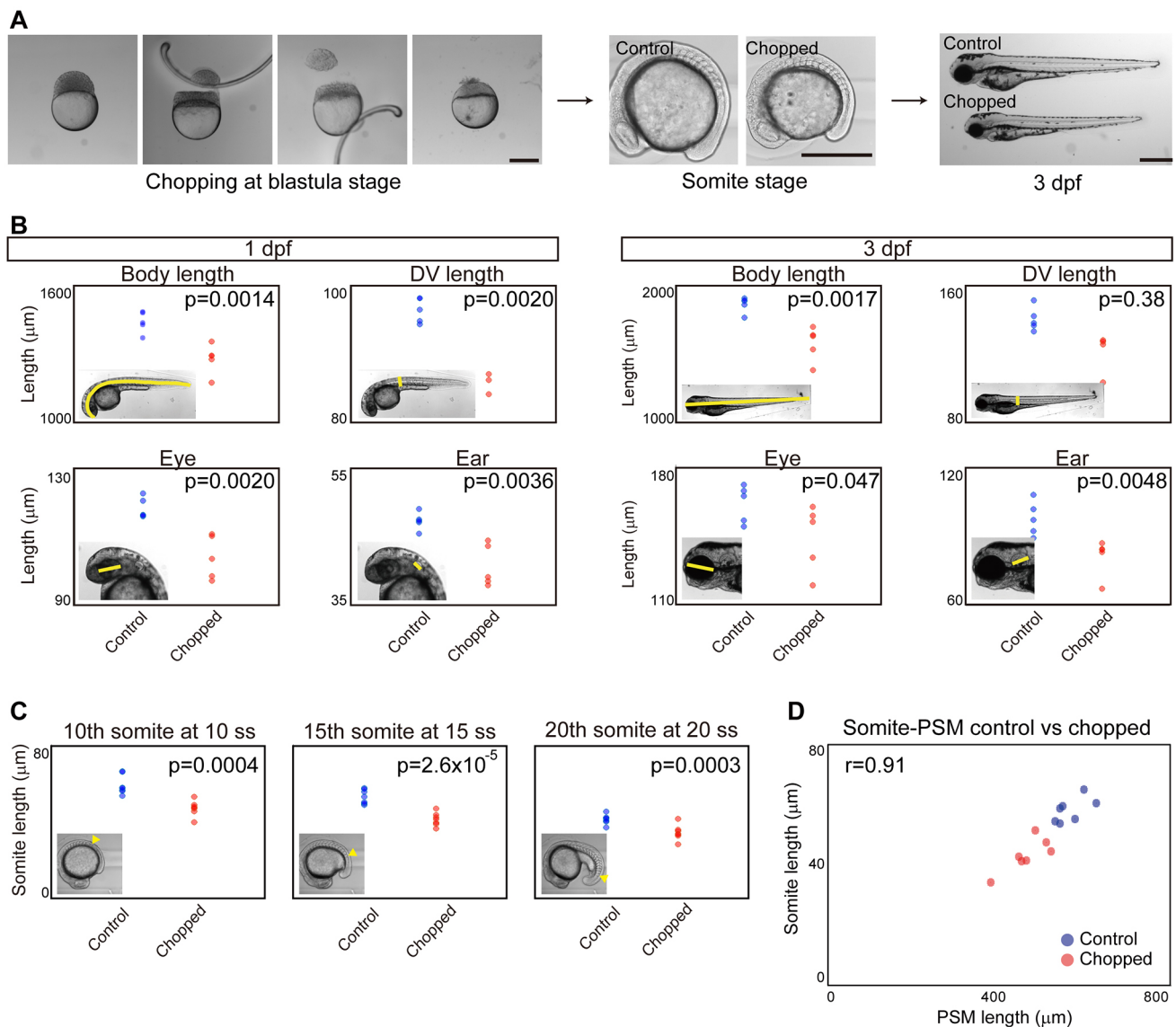


Fig. 2. Somite scaling between individuals of different sizes. (A) Size reduction technique. Scale bars: 500 μm . dpf, days post-fertilization. (B) Comparison of body and organ sizes between control and chopped embryos. Insets illustrate the region measured. $n=5$ each. (C) Comparison of somite size between control and chopped embryos. Somite of interest indicated by arrowhead in insets. $n=5$ each. (D) Somite size versus PSM size in control and chopped embryos. $n=7$ each.

scaling was observed throughout our time courses (from 5 ss to 20 ss; Fig. S3). Taken together, we conclude that somite length always scales with PSM length as long as the time delay between specification and morphological boundary formation is considered.

Clock period does not scale with PSM length

Given our finding that somite length scales with PSM length both over time and among individuals with different sizes, we next investigated what mechanism might link PSM size to somite size. For this purpose, we searched for a component of the known somite patterning system that scales with PSM length, both across developmental stages and among individuals. In the classic clock and wavefront model, somite length is the product of clock period and wavefront regression speed. We first measured the period of the segmentation clock in both control and chopped embryos over time, as it is known that a change in the period of clock gene expression causes a change in somite length (Harima et al., 2012; Herrgen et al., 2010; Schröter and Oates, 2010). We measured the clock period as the time between the formation of successive somite boundaries, and found that this period is similar and does not scale with PSM length between control and chopped embryos (Fig. 3A, Fig. S4) or between those at different developmental stages (Fig. 3B) (Schröter et al., 2008), suggesting that scaling is not achieved by regulation of clock period.

Axis elongation speed does not scale with PSM length

We next quantified the axis elongation speed, because slower axis elongation is known to lead to shorter somite length (Goudevenou et al., 2011; Rauch et al., 1997). One explanation for this comes from the clock and wavefront model, in which the wavefront speed (and hence somite size) has often been directly linked to axis elongation speed (Cooke and Zeeman, 1976; Dubrulle and Pourquié, 2004; Hubaud and Pourquié, 2014; Saga, 2012). This possibility is also consistent with the idea that a gradient of Fgf is established by mRNA decay coupled with axis elongation, and that this drives wavefront progression (Dubrulle and Pourquié, 2004). Therefore, we expected somites to be smaller in chopped embryos as a result of a decrease in the axis elongation speed (e.g. cells are incorporated into the PSM at the tailbud at a slower rate). We measured the change in axis length, defined by a distance between the posterior boundary of 4th somite and the tail tip, over time (Bajard et al., 2014). Contrary to our expectation, we found that axis elongation speed did not differ between control and chopped embryos, at least for 5ss-15ss (Fig. 3C, Fig. S4). This seemingly confusing result can be explained if the major mechanism of axis elongation at these stages is, for example, convergence and extension, the rate of which should not be size dependent (Steventon et al., 2016). Notably, the axis elongation speed was nearly constant over our experimental time window (Fig. 3D), although PSM size decreased drastically. Because axis elongation speed neither changes over time as somites decrease in size nor changes between embryos of varying sizes, altered axis elongation speed cannot explain scaling of somite patterning.

Wavelength of *her1* traveling waves does not scale with PSM length

We then investigated whether the wavelength of the traveling wave pattern of a segmentation clock gene (e.g. *her1*) could explain scaling of somite formation. Canonical segmentation clock genes exhibit traveling waves – a stripe pattern that sweeps through the PSM from posterior to anterior as a result of a phase delay toward

the anterior direction. Although these traveling waves have not been experimentally shown to cause somite size alterations, a correlation between wavelength (spatial interval of the stripes) and somite length has been observed (Jörg et al., 2016; Lauschke et al., 2013). To determine whether *her1* traveling waves are involved in scaling, we generated and quantified phase maps from *her1* *in situ* hybridization samples (Fig. 3E). We extracted the phase information from signal intensities using a wavelet transform, then converted the approximately linear phase gradient into an effective wavelength, defined as the distance between peaks of *her1* intensity (Fig. 3E). We measured the phase gradient from an area of PSM including B–4 (the presumptive position corresponding to a morphological boundary four cycles later; blue line in Fig. 3E, left). We also measured the phase gradient manually, by identifying peaks and troughs in the intensity profile (orange triangles in Fig. 3E, right). This manual measurement was found to correspond well with phases obtained from the wavelet transform (green line in Fig. 3E, right). We found that, unlike somite size, wavelength does not always scale with PSM size: although the wavelength scales with PSM size following embryonic size reduction, it does not scale during embryonic development (Fig. 3F,G) (Holley et al., 2000). This is consistent with recent work demonstrating that the number of *her1* waves changes over time, confirming that the phase gradient does not scale with PSM size (Soroldoni et al., 2014). Because somite size scales with PSM size over developmental stages as well as among individuals of different size, this result indicates that it is unlikely that the somite scaling is achieved through regulation of the wavelength of *her1*. This conclusion is supported by a previous study which showed that repeated induction of *deltaC* expression in a *deltaC* mutant background can successfully rescue somite boundary formation, although the induced *deltaC* expression did not show the traveling wave pattern (Soza-Ried et al., 2014).

The Fgf activity gradient scales with PSM length

Our final candidate feature that could relate somite size to PSM size was the Fgf gradient (Akiyama et al., 2014; Dubrulle et al., 2001; Sawada et al., 2001). To measure Fgf signaling, we used whole-mount immunohistochemistry against doubly phosphorylated Erk (dpErk), a downstream readout of Fgf activity, and extracted the signal intensity. We found that the gradient range varies considerably between embryos on an absolute length scale, but is consistent when plotted as a function of relative PSM length, both for control and chopped embryos (Fig. 3H,I, Figs S5 and S6) and for embryos at different developmental stages (Fig. 3J,K, Figs S5 and S6). We further tested whether Fgf activity scales with PSM size in embryos carrying a fluorescence resonance energy transfer (FRET)-based Erk biosensor (Fig. 3L-S). We calculated the PSM location at which the relative intensity of FRET signal crosses 50% of the maximal intensity (L50) (Fig. 3P). Recent work using the Erk live reporter showed that this L50 is a good approximation of the future somite boundary (Sari et al., 2018). Time course analysis of L50 in both control and chopped embryos confirmed that the Fgf activity gradient scales with PSM size (Fig. 3Q-S). L50 analysis was further performed when Fgf activity was measured by dpErk immunostaining and by *sprouty4* (a downstream gene of Fgf signaling) *in situ* hybridization, and also confirmed Fgf activity scaling (Fig. S7). Because Wnt signaling is also known to form a gradient in the PSM, we examined whether Wnt signaling scales with PSM length. We performed L50 analysis on expression patterns of *sp51* mRNA, a downstream target of Wnt signaling (Thorpe et al., 2005), and found that Wnt activity also scales with PSM length (Fig. S8).

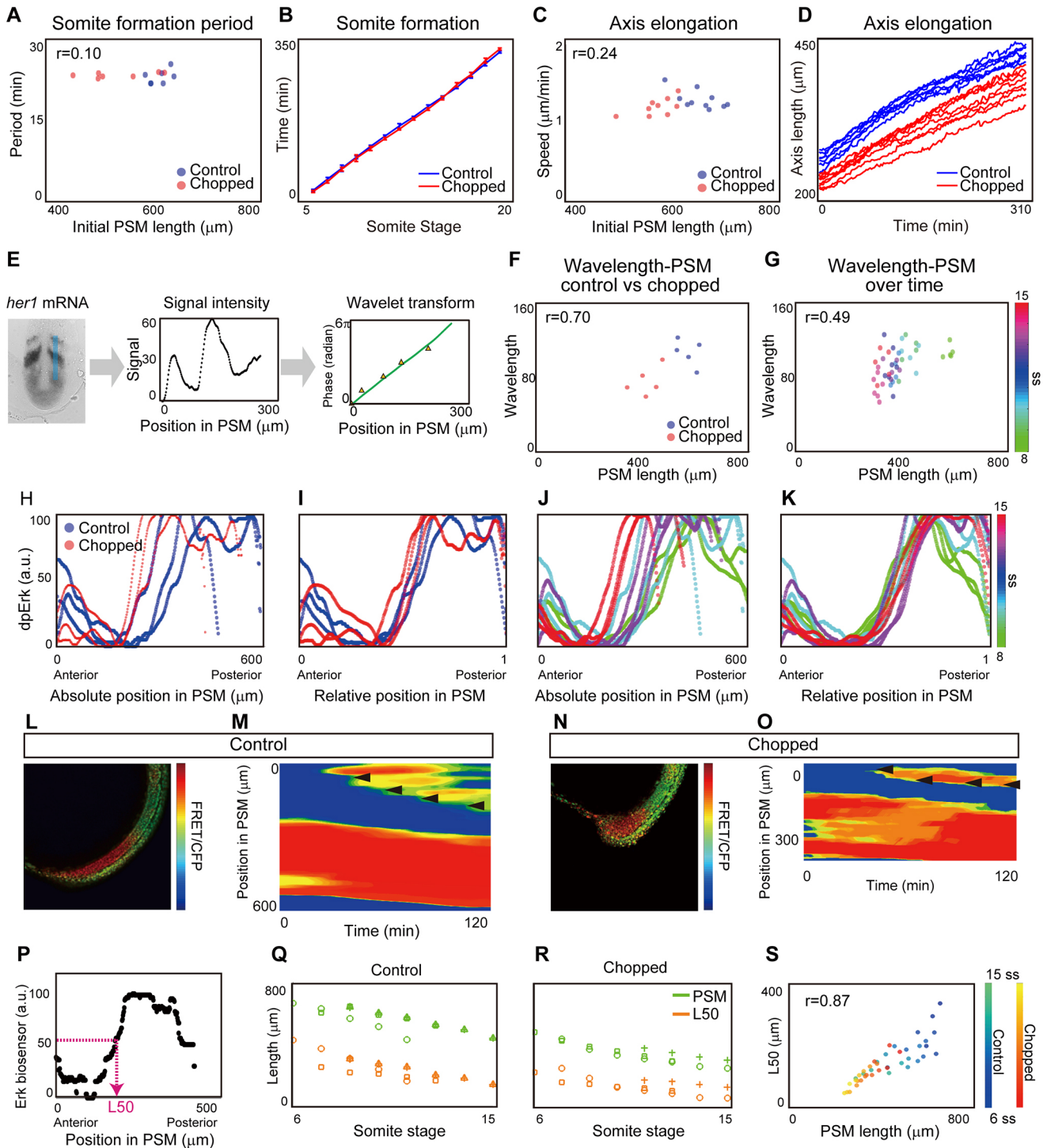


Fig. 3. Determining which components of the somite formation system scale. (A) Somite formation period versus initial PSM size. No significant difference was found between control and chopped embryos at the 5% significance level, and the confidence interval on the difference of means (-1.78 - 0.66) includes the hypothesized value of 0. $n=7$ each. (B) Somite formation time of control and chopped embryos. The slope corresponds to the somite formation period. Note that the slopes do not change over time. Error bars denote s.d. $n=7$ each. (C) Axis elongation speed versus PSM size. No significant difference was found between control and chopped embryos at the 5% significance level, and the confidence interval on the difference of means (-0.10 - 0.15) includes the hypothesized value of 0. $n=10$ for control, 9 for chopped. (D) Axis length versus time. The slope represents the speed of axis elongation. $n=10$ for control, 9 for chopped embryos. (E) Quantification of *her1* wavelength along the blue line in the first panel. Green line in the third panel shows the phase gradient obtained by wavelet transform. Orange triangles show manually measured wavelength. $n=5$ for each. (F) Wavelength versus PSM among individuals. $n=5$ for each. (G) Wavelength versus PSM size over time. Colors denote somite stage as indicated by the scale. $n=5$ - 7 for each time point. (H-K) Quantification of Fg activity based on dpErk immunostaining. (H,I) dpErk scaling between control and chopped embryos. $n=3$ for each. (J,K) dpErk scaling across developmental stages. $n=3$ for each time point. Both are shown by absolute position (H,J), and relative position (I,K). (L-S) Quantification of Fg activity based on Erk biosensor mRNA-injected embryos. The manipulated embryos (L,N) were used to generate kymographs of Erk activity (M,O). Black arrowheads indicate newly formed somites. Color scale indicates high (red) to low (blue) reporter intensity. (P) Definition of L50. (Q,R) Change in PSM size and L50 position over time in control embryos (Q) ($n=4$) and chopped embryos (R) ($n=3$). Different symbols correspond to different individual embryos measured at multiple stages. (S) L50 vs PSM length over time both in control and chopped embryos. $n=4$ for control, 3 for chopped.

A clock and scaled gradient model can explain somite scaling

Given our observation of a dynamically scaling gradient, we turned to modeling to determine whether this feature is capable of explaining scaling of somite patterning. In the original clock and wavefront model, the timing of somite boundary specification is controlled by a clock and the positioning by the level of a signal that encodes a posteriorly moving wavefront. How the position of the wavefront is determined at each time point is unspecified in the original model. Importantly, our observations reveal that the activity of signaling molecules linked with wavefront activity forms a dynamic gradient that scales with PSM size. We term this updated model the ‘clock and scaled gradient’ model. In this model, scaling of the gradient to PSM size generates a posteriorly moving wavefront, which is combined with axis elongation (which increases PSM size) and somite formation (which decreases PSM size) (Fig. 4A,B). We constructed a simple mathematical model to formalize these interactions (supplementary Materials and Methods) and found that this model can successfully reproduce our biological results on somite size scaling (Fig. 4C-F, Movie 1). Similar somite formation dynamics can be observed regardless of the precise shape of the gradient (Fig. 4C,D, steep sigmoidal gradient; Fig. 4E,F, linear gradient). Interestingly, we also observed step-wise rather than continuous regression of the L50 in our model (Fig. 4G, H), consistent with recent results (Akiyama et al., 2014). Moreover, using this model, we can also accurately predict the resulting changes in somite size following a wide range of additional previously published perturbations (Fig. 4I,J): one smaller somite following transient Fgf activation (Akiyama et al., 2014) (Fig. 4I); multiple smaller somites followed by one larger somite after Fgf bead transplantation (Dubrulle et al., 2001; Sawada et al., 2001) (Fig. 4I); larger somites with a slower clock (Herrgen et al., 2010; Kim et al., 2011; Schröter and Oates, 2010) (Fig. 4I); smaller somites with slower axis elongation (Goudevenou et al., 2011; Rauch et al., 1997) (Fig. 4I); and scaling of somite and PSM size *in vitro* under culture conditions that do not permit axis elongation (Lauschke et al., 2013) (Fig. 4J). We found that in all cases, the model’s predictions were in agreement with experimental results.

The clock and scaled gradient model predicts one larger somite in long-term Fgf inhibition

A simple perturbation to test our model is long-term Fgf inhibition. This experiment was recently carried out using chick embryos and multiple larger somites were shown to form during long-term Fgf inhibition (Cotterell et al., 2015). This result was contradictory to what the clock and wavefront model would predict, but consistent with a novel Turing framework for somitogenesis (Cotterell et al., 2015). We simulated the same perturbation using our clock and scaled gradient model and found that it predicts the same result as the clock and wavefront model: only one larger somite (Fig. 4I,K). To test whether long-term Fgf inhibition has the same effect in zebrafish embryos, we treated zebrafish embryos with the Fgf inhibitor SU5402 (Sawada et al., 2001) at a low concentration (16 μ M) and allowed the embryos to grow until late stages under this condition. Unlike in chick (Cotterell et al., 2015), we observed one larger somite but not multiple larger somites following long-term SU5402 treatment (Fig. 4L,M, Fig. S9; for individual data, see Fig. S13), consistent with our model. Moreover, in 10 out of 11 embryos we observed the same tendency under constant darkness, confirming that the result we obtained was not due to the light instability of SU5402 (Fig. S10). These differences in results could potentially be explained by how acutely the drug can be

administered: in zebrafish, embryos can be soaked in a vast excess of the drug causing a rapid step-up in drug levels followed by a plateau *in vivo*, whereas in chick the drug levels may rise more slowly. Simulations showed that increasing Fgf inhibition over a few hours can cause multiple large somites in our model (Fig. S11).

Newly formed somites play a crucial role in gradient scaling

One potential mechanism of gradient scaling is that newly formed somites modulate the gradient, for example by secreting a negative regulator. To examine whether the newly formed somite can modulate the gradient, we transplanted a newly formed somite into the posterior PSM, and compared it with a control experiment in which PSM cells were transplanted to the same axial level (Fig. 5A). From our model, we predicted that the ectopically transplanted somite would locally inhibit Fgf signaling. One to two cycles (0.5–1 h) after transplantation, the embryos were fixed and stained for dpErk. We found that in the PSM surrounding the transplanted somite, the dpErk level was significantly decreased (Fig. 5B), whereas the dpErk level in the PSM surrounding transplanted PSM cells was largely unaffected (Fig. 5C). To quantify Erk activity, we normalized the dpErk signal near the transplant with that of the non-transplanted side of the same embryo at the same axial level (Fig. 5A). We found the dpErk levels around the transplanted somite to be significantly lower than the control (Fig. 5D). These data support our hypothesis that mature somites rapidly and potently modulate the Fgf activity gradient to effect gradient scaling.

A unique prediction from the clock and scaled gradient model: an ‘echo effect’ on somite size

We next sought a novel experimental test for which our model makes a unique prediction. Key aspects of the clock and scaled gradient model are the 4-cycle delay between somite specification and formation, and the feedback between newly formed somites and gradient length. We thus reasoned that if we created one larger somite experimentally, it would shorten the PSM and rescale the gradient in a jump, which would then result in another larger somite four cycles later, and this process would repeat creating ‘echoes’ of larger somites with a \sim 4-cycle periodicity (Fig. 6A). Simulations of our model supported this idea (Fig. 6B,C).

To test this prediction, we treated embryos transiently with the Fgf inhibitor SU5402, which is known to induce a larger somite (Dubrulle et al., 2001; Sawada et al., 2001), followed by extensive washes for two hours, then performed live imaging to measure the length of the newly formed somites (Fig. 6D). Strikingly, we found that somite size became alternately smaller and larger with a several-cycle period, which was uniquely predicted by the clock and scaled gradient model (Fig. 6E,F; for individual data, see Fig. S12). We noted that the periodicity was not always precisely four (Fig. 6F), possibly owing to internal fluctuation of the delay time or experimental variation, such as variation in washout timing of SU5402. By analyzing individual embryos (Fig. S12), we confirmed that all the peaks of somite size in pulse SU5402-treated embryos are larger than those in control embryos (Fig. 6G). Our model also predicts the echo effect for long-term SU5402-treated embryos, which we confirmed experimentally (Fig. S13), but we chose to focus on transient treatment because the embryos are healthier. The echo effect was also seen in embryos transiently treated with BCI (Fig. S14). These results confirm that the echo effect is a general phenomenon for somite formation. We note that a potentially related phenomenon has been seen following heat-shock in chick and zebrafish (Primmitt et al., 1988; Roy et al., 1999) but through an unclear mechanism.

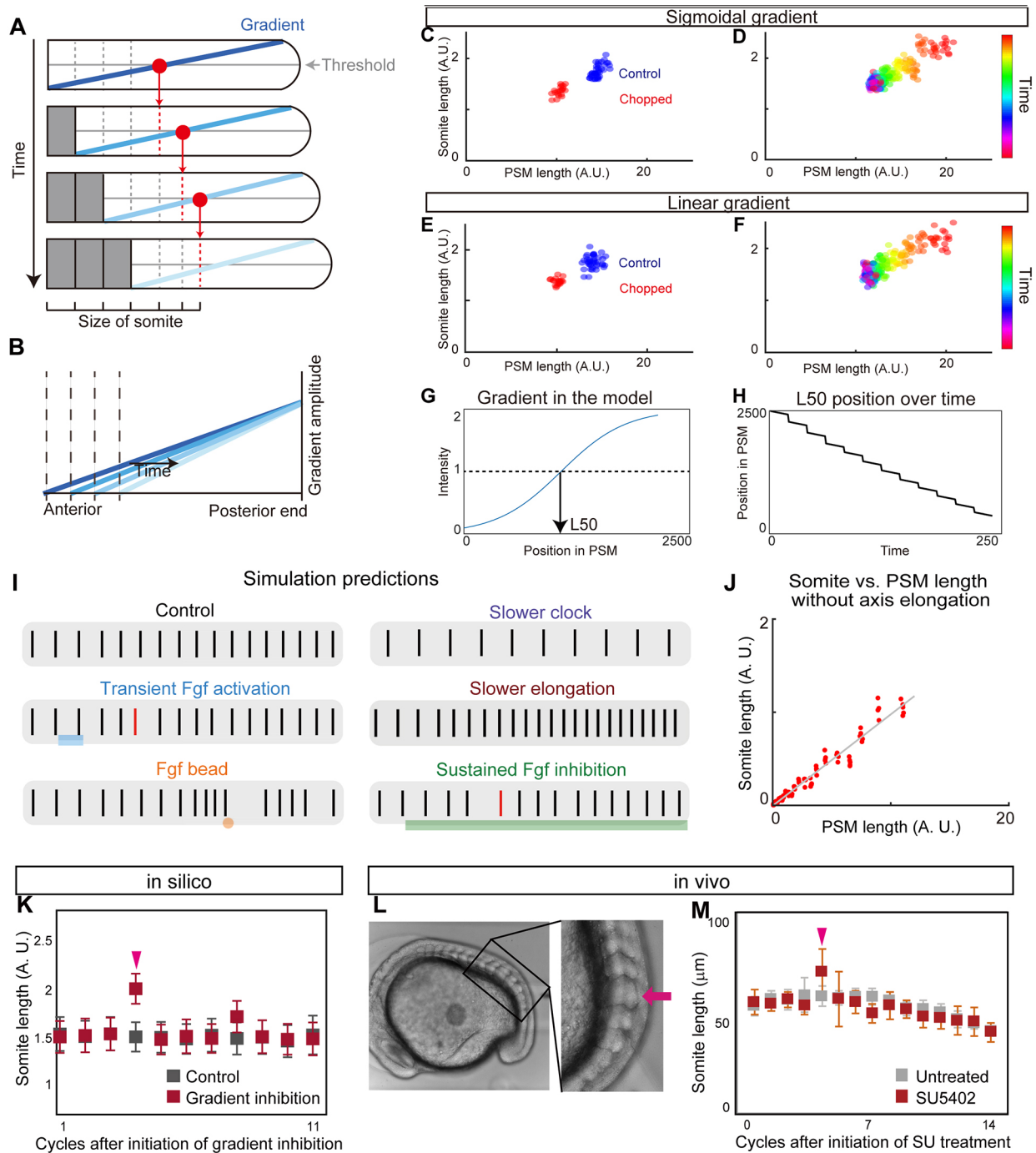


Fig. 4. Clock and scaled gradient model. (A) Schematic of the clock and scaled gradient model. The position of a future somite boundary is set by a scaled gradient once per clock cycle (each row) and the boundary appears after a delay. (B) Superimposition of the gradients from each time point shown in A. (C,D) Simulation results using a sigmoidal gradient. (E,F) Simulation results using a linear gradient. (C,E) Simulation results of control and chopped embryos. (D,F) Simulation results of a single embryo over time. (G,H) Stepwise regression of the gradient in clock and scaled gradient model. (G) L50 in the model was determined similarly to Fig. 3P. (H) Clock and scaled gradient model predicts stepwise regression of L50 position. (I) Simulation results for perturbation experiments for local or global inhibition/activation of Fgf, slower clock and slower axis elongation. Black vertical lines represent simulated somite boundary positions. (J) Somite size versus PSM length shows perfect scaling *in silico* when axial elongation speed is zero, mimicking the results from the *in vitro* mPSM system (Lauschke et al., 2013). (K) Simulation results of long-term suppression of a gradient in the clock and scaled gradient model. Error bars denote s.d. (L,M) Treatment with a low concentration of SU5402 (16 μ M) results in one or two larger somite(s) (arrow) ($n=7$ for both SU5402 and untreated groups). Error bars denote s.d.

We next evaluated the effect of transient SU5402 on both dpErk activity and *her1* wavelength (Fig. 6H-K; for individual dpERK data, see Fig. S15). To perform time-course analysis, we fixed embryos every 30 min following SU5402 treatment (Fig. 6H). dpErk immunostaining showed that maximal Fgf activity recovered

quickly after SU5402 treatment, confirming that the inhibitor is rapidly washed out (Fig. 6I). We then examined later time points, when we expected the secondary ‘echo’ effect to be seen, and, as predicted, the dpErk activity was found to scale with the induced smaller PSM (Fig. 6J). In contrast, we found no significant

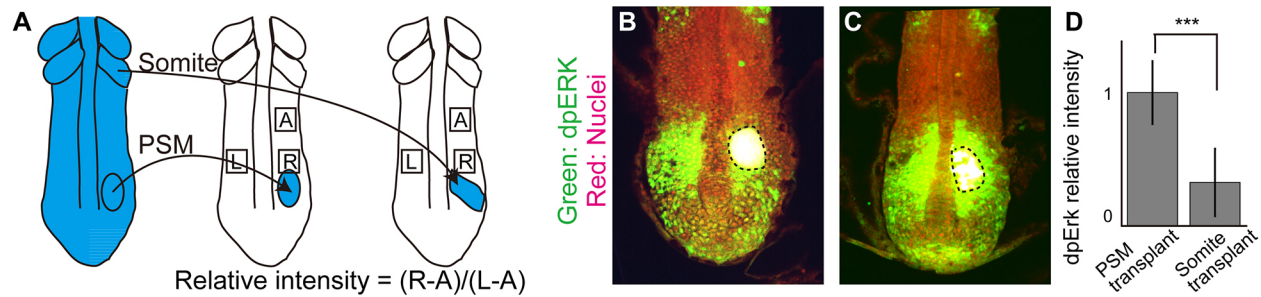


Fig. 5. New somites inhibit Fgf activity. (A) Schematic of somite transplantation. (B,C) dpErk immunostaining. Dashed line encircles transplanted tissue. (D) Comparison of relative intensities between PSM-transplanted samples ($n=9$) and somite-transplanted samples ($n=9$). Error bars denote s.d. $***P < 0.001$.

difference in *her1* wavelengths between control and SU5402-treated embryos (Fig. 6K), suggesting that gradient scaling, and not *her1* waves, are responsible for the echo effect.

This echo effect is only predicted if the ‘specification position’ of new somites (rather than the somite itself) scales with PSM size, which is the core assumption of the clock and scaled gradient model (Fig. 6L–N). Without gradient scaling, the clock and wavefront model predicts a single smaller somite following the induced larger somite, but the size of the following somites immediately returns to normal (Fig. 6L), consistent with previous theoretical work (Baker et al., 2006). Interestingly, for a class of mechanisms that assumes that the ‘size’ of a somite is what is determined, rather than the ‘position’ of the next somitic furrow (e.g. somite size is determined by the wavelength of traveling waves, or the wavelength of a Turing-type pattern), then the predicted result is qualitatively different (Fig. 6M). In these models, somite size scales with the smaller PSM resulting from the induced larger somite, and then somite size gradually goes back to the normal size without rebounding dynamics. The clock and scaled gradient model provides an alternative scenario that is uniquely supported by our experimental tests.

Traveling waves have a minor effect in the clock and scaled gradient model

Spatial differences in the phase of the coupled oscillators comprising the segmentation clock give the appearance of traveling waves of clock gene expression in the PSM from posterior to anterior (Ares et al., 2012; Ay et al., 2014; Giudicelli et al., 2007; Morelli et al., 2009; Uriu et al., 2009), but a mechanistic role for these waves is unclear. Consistent with previous theoretical work (Ares et al., 2012; Morelli et al., 2009), our simulations show that traveling waves arise in systems of coupled oscillators under a wide variety of conditions, including spatial variation in intrinsic frequency, coupling strength, and coupling phase delay, as well as differences in boundary conditions (Fig. S16), and thus their existence may not be significant. Thus far, we have assumed synchronous oscillations throughout the PSM in our model for simplicity, as was done in the original clock and wavefront model (Cooke and Zeeman, 1976). To determine whether traveling waves affect the clock and scaled gradient model, we assumed a simple linear phase gradient along the anteroposterior (AP) axis that approximates the *in vivo* phase gradient (for details, see supplementary Materials and Methods) and repeated the simulations. As shown in Fig. 7A, this results in only a minor modification to somite sizes compared with a model without a phase gradient. Interestingly, we noticed that the somite formation period (defined as the time between successive boundaries being specified) was smaller when including a phase gradient (Fig. 7B). This is consistent with the observation of the segmentation period in

zebrafish being slightly faster than the intrinsic clock period – a phenomenon likened to the Doppler effect (Soroldoni et al., 2014), in which an observer moving towards a source of traveling waves measures a higher frequency than the intrinsic frequency of the oscillators. We suggest that this effect is caused by the wavefront moving towards the tailbud during development owing to gradient scaling as the PSM shrinks rather than a change in arrival time of traveling waves to the anterior boundary (Fig. 7C). These results show that (1) phase gradients have only minor effects on the clock and scaled gradient model and that (2) a model not based on traveling waves can also explain the Doppler effect.

DISCUSSION

Here, we have proposed a novel mechanism for somitogenesis: the clock and scaled gradient model. This model is based on the original clock and wavefront model but (1) the wavefront specifies new somite boundaries at a fixed relative position along the PSM as a result of gradient scaling, and (2) there is a delay between somite boundary specification and formation. Previously, multiple models of somitogenesis have been proposed, but were difficult to distinguish experimentally as they were all consistent with existing data from wild-type embryos as well as existing experimental perturbations. Here, we utilized a novel perturbation – changing system size – to discriminate between existing models, and showed that only the clock and scaled gradient model can explain existing data and our new experimental data. We found that in patterning of the somites, somite length scales with PSM length *in vivo*. Importantly, we demonstrate that the delay between somite boundary specification and formation is crucial for examining the relationship between somite and PSM length. This is because the change in PSM length (and, as a result, somite length) is dynamic, owing to the changing rates of PSM production by axis elongation and consumption by somite formation (Fig. 1G). Consistently, when the PSM is grown in culture conditions that do not permit axis extension, there is a monotonic decrease in PSM size and somite-PSM scaling is observable without considering the delay (Lauschke et al., 2013). Considering the delay time between somite boundary specification and the appearance of a morphological somite will be essential for studying somite scaling in other situations, such as in other species, in which complex dynamics of PSM length can be observed (Gomez et al., 2008; Schröter et al., 2008).

The clock and wavefront model is the classic model for somitogenesis (Cooke and Zeeman, 1976) and explains a number of previous experimental observations. In the original clock and wavefront model, what controls wavefront progression and how it is linked to axis elongation is unspecified. A simple and widely accepted way to specify wavefront progression is to tie it just to axis elongation (Cooke and Zeeman, 1976; Dubrulle and Pourquie,

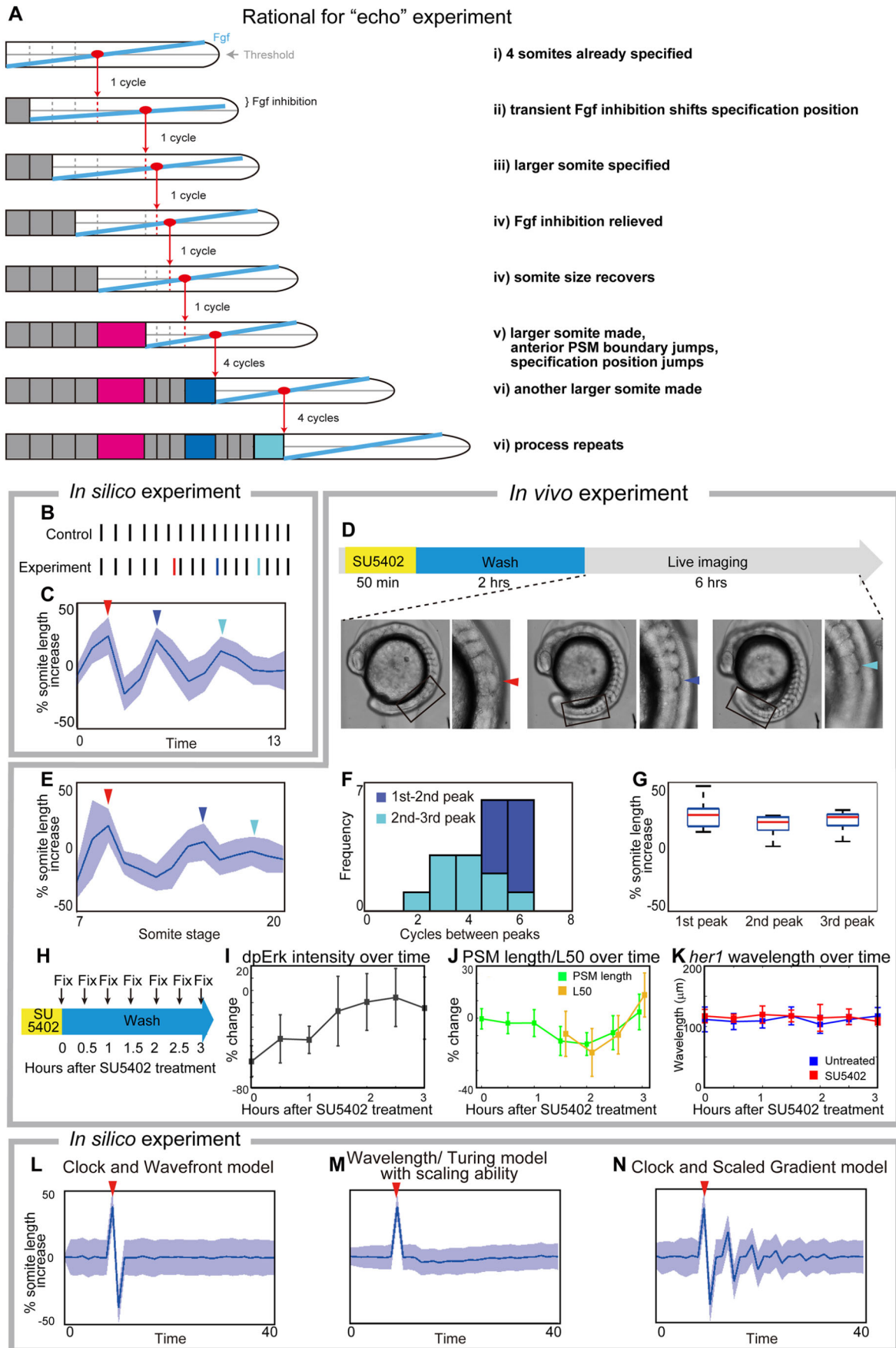


Fig. 6. See next page for legend.

Fig. 6. Experimental validation of the clock and scaled gradient model.

(A) Schematic of the outcome of the clock and scaled gradient model, following induction of one larger somite. The induced larger somite is magenta, and the larger somites as a result of system response are blue and cyan. (B,C) Simulation results without (B) and with (C) noise for somite size (red line in B, red arrowhead in C). Blue line in B and blue arrowhead in C show the second, and cyan line in B and cyan arrowhead in C show the third large somite. (D) Schematic of the *in vivo* experiment, and an embryo with larger somites at different time points. Boxed areas are shown at higher magnification to the right with arrowheads indicating the larger somite. (E) Time course of percentage increase in somite length of SU5402-treated embryos, compared with those in control embryos ($n=12$). (F) Frequency distribution of somite cycles between the peaks. (G) Percentage increase in somite size in SU5402-treated embryos at the peaks detected in each embryo, compared with control embryos at the corresponding somite stage. In both C and E, blue lines and blue shades indicate the average somite size and the variance of one standard deviation, respectively. For C-E, red, blue and cyan arrowheads show the first, second and third larger somites, respectively. (H-K) Examination of Erk activity ($n=6$ for each time point) and *her1* wavelength ($n=4-8$ for each time point) after transient SU5402 treatment. Error bars denote s.d. (H) Schematic of the experiment. After fixation, the samples were subjected to dpErk immunostaining and *her1* *in situ* hybridization. (I) Time course of percentage change in dpErk maximum intensity in SU5402-treated embryos, compared with that in control embryos. (J) Time course percentage change in PSM size and L50 position in SU5402-treated embryos, compared with those in control embryos. Note that L50 analysis begins 1.5 h after SU5402 treatment when dpErk intensity has recovered (see Fig. 6I) because it cannot be defined earlier. (K) Time course analysis of *her1* wavelength of untreated embryos and SU5402-treated embryos. We found no significant difference (significance threshold $P<0.05$) at any time point. (L-N) Simulation results for percentage increase of somite size over time, based on different models. After induction of one larger somite (arrowheads), the clock and wavefront model (when wavefront speed is associated with axis elongation only) predicts one smaller somite (L), the wavelength/Turing model (Cotterell et al., 2015) predicts smaller somites and the somite size eventually comes back to normal (M). Only the clock and scaled gradient model predicts the ‘echo effect’ that somite size dynamics oscillate repeatedly every four cycles (N).

2004; Hubaud and Pourquie, 2014; Saga, 2012). The consequence of tying wavefront speed only to axis elongation is that somite size is equal to how far the tail moves in one clock cycle; it could still

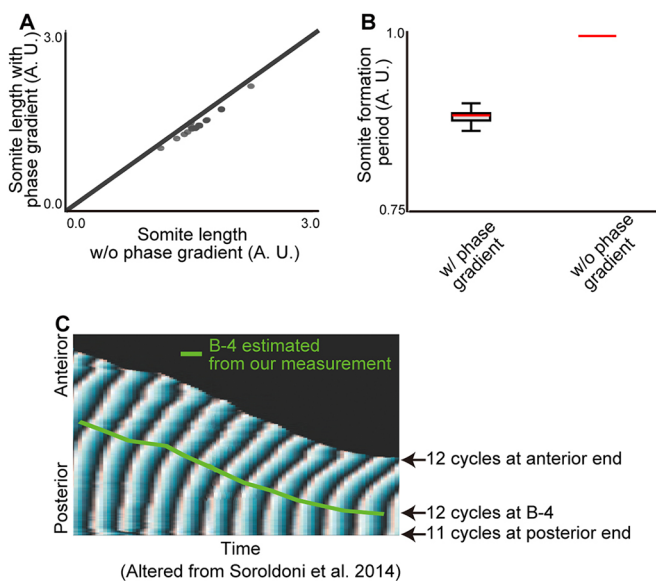


Fig. 7. Traveling waves have modest effects on the clock and scaled gradient model. (A) Somite sizes are only slightly changed (~9%) by the presence of a phase gradient. (B) The phase gradient decreased the segmentation period (~11%). Error bars denote s.d. (C) B-4 positions estimated by our measurement are superimposed with the phase map generated previously (Soroldoni et al., 2014).

explain somite scaling if axis elongation speed scaled with PSM size, but we found that is not the case (Fig. 3C,D). Additionally, in the absence of axis elongation no somites should form, but this prediction is contradicted by *in vitro*-cultured PSM, which has no axis elongation yet forms a series of progressively smaller somites (Lauschke et al., 2013). Similarly, this simple clock and wavefront model does not predict the non-monotonic somite size variations following induction of a single large somite, as seen in Fig. 6, because perturbations to the anterior PSM should not affect wavefront position.

An alternative class of models for explaining somite formation is based on use of the wavelength of traveling waves to determine somite size (Jörg et al., 2015, 2016; Lauschke et al., 2013). However, previous studies, in addition to our new results, suggest that the wavelength of the traveling waves is not the primary mechanism responsible for setting somite size. First, the simple scenario (Lauschke et al., 2013) assumes that the phase gradient (inverse of wavelength) of the entire PSM scales with PSM length and that the scaled wavelength sets the somite size. However, previous results (Soroldoni et al., 2014) and our results show that the phase gradient does not always scale with PSM length, which argues against this simple mechanism. Second, one could still imagine some modification of the simple wavelength model could explain the *in vivo* situation of somite scaling (e.g. the wavelength at B-4 locally scales with PSM length). However, this model is still hard to reconcile with the echo effect we observed after inducing one large somite (Fig. 6) because, regardless of the details, this class of models assumes that somite ‘size’ (not somitic furrow position) is controlled by the wavelength. In Fig. 6M, we explicitly model the case in which somite sizes scale with PSM size (including the 4-cycle delay) and find that it cannot explain the echo effect. In order to directly test whether traveling waves are functional, one should experimentally modify the spatial pattern of the waves (for example, by changing or eliminating the spatial phase gradient), without affecting the intrinsic period of the oscillators (Soza-Ried et al., 2014), and a mechanism for detecting a spatial gradient in clock gene expression level should be proposed. We suggest that traveling waves could be a byproduct of the need to synchronize oscillators locally (within the spatial scale of a somitic furrow), and that, although visually striking and mathematically interesting, they have only a peripheral role in somite formation.

Another type of model is ‘Turing-like’, in which somites are formed by a combination of an oscillator and a periodic Turing instability (Cooke and Zeeman, 1976; Cotterell et al., 2015). There are several reasons why our data do not support Turing-like models. First, a recent paper (Cotterell et al., 2015) showed how a Turing-like model of somitogenesis could, in principle, explain somite scaling, if one allowed the level of Fgf to effectively modulate the Turing spacing of the somites. However, the change in somite size in response to PSM length is small, and is inconsistent with our *in vivo* measurements, which showed that somite length is almost proportional to PSM length (Fig. 1F, Fig. 2D). A second argument against a Turing-like model is that, unlike the clock and wavefront and clock and scaled gradient models, the ‘clock’ is not separable from the other components in the system. Therefore, we do not necessarily expect a slower clock to increase somite size, at least not in perfect proportion as has been observed *in vivo* (Herrgen et al., 2010; Kim et al., 2011; Schröter and Oates, 2010), because a change in clock period would be associated with other parameters. Third, the assumption that Fgf modulates the Turing spacing of somites is incompatible with the Fgf perturbation results, specifically: (1) a Turing-like model

predicts consistently larger somites following sustained Fgf inhibition, which we do not see (Fig. 4L,M); (2) a Turing-like model predicts a symmetric effect of implanting a Fgf bead (i.e. smaller somites both anterior and posterior to the bead) unlike *in vivo* observations, which show a definite anterior-posterior bias (Dubrulle et al., 2001; Sawada et al., 2001); and (3) it is difficult to reconcile a Turing-like model with the echo effect (Fig. 6). The reason is that, like the phase-gradient model and unlike the clock and scaled gradient model, Turing-like models fundamentally control somite size, not somite boundary position. Therefore, for exactly the same reasons as argued for the phase-based models, even with perfect somite size scaling in wild-type embryos, Turing-like models do not predict the non-monotonic segment size variation observed following transient Fgf inhibition.

The clock and scaled gradient model presented here is a fairly simple model. We used a simple model for three reasons: (1) so that the key assumptions of the model (clock+scaling gradient) are directly supported by experimental data; (2) so that the model is at the right level of detail to make comparisons to our data; and (3) so that the model gives us a qualitative and intuitive understanding of somite size control, which could be obscured in a more complex model (Gunawardena, 2014). However, the simplicity of the model does mean that it should not be viewed as a comprehensive, or completely realistic, model of somitogenesis. First, we have assumed that somite maturation, and its effects on gradient scaling, occur instantly, whereas in reality we expect this to be a more gradual effect. Mathematically, this might mean that the 4-cycle delay should be changed from a step function to a more slowly varying function. This modification may be particularly important to understand the formation of the first four somites, and to reduce the sensitivity of somite size to initial conditions and/or perturbations. A second shortcoming of our model is that we have chosen the somite boundary to be set by a simple threshold of the gradient, an assumption that has not been directly measured and is likely a simplification. Third, we have largely focused on dpErk as readout of wavefront activity and demonstrated dpErk scaling as a proof of concept. However, the wavefront could be set by a complex function of multiple inputs, such as Fgf and Wnt along with downstream signal integration (Bajard et al., 2014; Stulberg et al., 2012; Wahl et al., 2007), without affecting the core conclusions of our model. As reported, dpErk shows a steep gradient (Akiyama et al., 2014), but in our model, similar somite formation dynamics can be observed regardless of the precise shape of the gradient; even a simple linear gradient can recapitulate the *in vivo* behavior rather closely (Fig. 4E,F). Finally, the molecular mechanism of gradient scaling remains to be determined. Numerous regulatory interactions have been shown in the posterior axis between Fgf, Wnt, Brachyury, Sprouty and Retinoic Acid so these are all candidates (Diez del Corral et al., 2003; Olivera-Martinez and Storey, 2007).

One reason we chose to look at scaling of somites in size-reduced embryos is that we thought we might discover a mechanism for scaling that is not based on scaling of a molecular gradient (e.g. change in axis extension speed, growth rate, phase gradient, oscillation period). However, in the end we found that scaling of a molecular gradient is indeed what underlies somite scaling, as has been observed in other examples of pattern scaling (Ben-Zvi and Barkai, 2010; Howard and ten Wolde, 2005; Umulis and Othmer, 2013). Future research on this issue could reveal the design benefits (e.g. robustness, evolvability) that systems employing gradient scaling have compared with other potential mechanisms for scaling.

MATERIALS AND METHODS

Fish care

Fish (AB) were kept at 27°C on a 14-h light/10-h dark cycle. Embryos were collected by natural crosses. All fish-related procedures were carried out with the approval of the Institutional Animal Care and Use Committee (IACUC) at Harvard University.

Size reduction technique

Chorions were enzymatically removed using pronase (Sigma-Aldrich, 1 mg/ml in egg water; Westerfield, 2000) at the ~512 cell stage. Eggs were treated with pronase until the chorions lost their tension and were then washed gently with egg water. Remaining chorions were removed manually using tweezers. The embryos were placed on a glass dish with 1/3 Ringer's solution (Westerfield, 2000), with 2% methylcellulose (Sigma-Aldrich) in 1/3 Ringer's solution spread thinly on the bottom of the dish, to restrict the movement of embryos. We found that using 1/3 Ringer's solution is essential for embryos to recover from the damage of chopping. Then, the blastoderm was chopped at the animal pole, and the yolk was wounded, resulting in oozing out of the yolk, using either a hand-pulled glass pipette or a looped stainless steel wire (30 µm in diameter) glued in the capillary glass. The chopped embryos were incubated in 1/3 Ringer's solution for 30 min, and then moved to fresh 1/3 Ringer's solution for further incubation. The survival rate of the chopped embryos varied depending on the condition of the embryos. Healthy embryos and good dissection would give ~60% success rate as measured by normal development until late stages (at least several days). The ratio of remaining cells and yolk affects how well the embryos develop; usually cutting horizontally at the 50% position in the animal-vegetal axis of the blastula and wounding the vegetal part of the yolk produced good results.

BCI and SU5402 treatment

Embryos were treated with BCI (Dual Specificity Protein Phosphatase 1/6 Inhibitor, Calbiochem) as described (Akiyama et al., 2014). For SU5402 (Calbiochem) treatment, embryos were treated with a low concentration (16 µM) to minimize toxicity.

Imaging

For live imaging, embryos were mounted laterally using the dorsal mount (Megason, 2009) in egg water with 0.01% tricaine (Western Chemical). Live imaging was performed using a Zeiss Axio Observer Z1 and AxioCam MRm. For multiple image acquisition, we used a motorized stage, controlled by AxioVision 4.8. The temperature was maintained at 28.5±0.5°C using a home-made incubator. The images were taken every 2 min, and the size of z-slices varied depending on the size of embryos. Images of the *in situ* hybridization samples were also acquired using a Zeiss Axio Observer Z1. Images of dpErk immunostaining samples were acquired using a Leica TCS SP8. Finally, a Nikon Ti spinning disk confocal was used to acquire the images of transplanted samples.

Image processing

Image processing was carried out using Fiji (Schindelin et al., 2012) and Matlab custom code. For time course measurement of axis elongation and somite size, we used the Gaussian-based stack fuser in Fiji. For axis elongation measurement, the length from the fourth somite to the tail tip was measured, using Fiji's LOI interpolator. For *in situ* hybridization samples and immunostaining samples, noise was first reduced using Gaussian blur ($\sigma=7.0$), and the signal was extracted along AP axis, using Fiji's 'Plot profile' function. To compare intensity profiles of BCI- and SU-treated embryos (Figs S1 and S9), we averaged over multiple embryos. To calculate relative intensity, the minimum value was first set to 0 and then the intensities at each position were scaled with a scaling factor of the average maximum intensity in drug-treated embryos divided by the average maximum intensity of untreated embryos.

In situ hybridization and immunostaining

In situ hybridization was performed as previously described (Nikaido et al., 1997). dpErk immunostaining was performed following the protocol described by Sawada et al. (2001), except that we used Alexa Fluor

488-conjugated goat anti-mouse IgG (Thermo Fisher Scientific, A-11001) as the secondary antibody. Nuclei were stained with propidium iodide (Life Technologies, P1304MP).

Somite/PSM transplantation

Transplantation was performed as described (Haines et al., 2004; Kawanishi et al., 2013), with minor modifications. For making a cut on the skin, we used a mouth pipette filled with pancreatin, so the cut can be made both physically and enzymatically. Embryos for donor tissue were injected with Alexa Fluor 680-conjugated 10,000 MW Dextran (Thermo Fisher Scientific, D34680), which can be detected directly after immunostaining.

Live imaging of Erk activity dynamics

The FRET-based Erk biosensor termed Eevee-ERKns is composed of an enhanced cyan-emitting mutant of GFP (ECFP), a WW domain (ligand domain), an EV linker, an Erk substrate (sensor domain), a yellow fluorescent protein for energy transfer (Ypet), and a nuclear localization signal (NLS) (Komatsu et al., 2011). When Erk phosphorylates the Erk substrate, the WW domain binds to the Erk substrate, leading to the induction of FRET from ECFP to Ypet. It has been confirmed that the Erk biosensor can monitor Fgf-dependent Erk activity in living zebrafish embryos (Sari et al., 2018). One-cell-stage embryos were injected with mRNA encoding a FRET-based Erk biosensor termed Eevee-ERKns (Sari et al., 2018; Komatsu et al., 2011). The embryos at a certain stage were excited with a 440-nm laser, and fluorescence spectra were acquired using the ‘Lambda scanning’ mode of a LSM710 confocal microscope (Zeiss). Using the ‘linear unmixing’ mode, CFP and Ypet signals were separated from the original spectra data. FRET/CFP ratio images and kymographs were created with MetaMorph software (Molecular Devices).

Statistics

Significance was calculated using one-tailed Student’s *t*-tests in Excel (Microsoft). Unequal variance comparison was performed for Fig. 1D and Fig. 2B,C, and equal variance comparison was performed for Fig. 5D and Fig. 6K.

Wavelet transform

We followed the approach of Soroldoni et al. (2014) and use the wavelet transform to generate phase maps for *her1* along the embryo. Consider that the *her1* pattern is of the form:

$$h(x) = h_0 + A(x)\sin(\phi(x) + \Phi)$$

i.e. has a spatially varying amplitude, $A(x)$ and a spatially varying phase, $\phi(x)$. By performing a wavelet transform, we can convert the intensity profile $h(x)$ into an effective phase profile $\phi(x)$, plotted in Fig. 3E. Note that we plot the phase for positions more anterior than the first clear peak because only in these ranges is there a distinct spatial pattern above noise, and, in all cases, this phase contains the position at which the next somite boundary is specified i.e. B-4. We also measured the phase gradient manually, by identifying peaks and troughs in the intensity profile (separated by π). This manual measurement (Fig. 3E, orange triangles) was found to match the corresponding phases obtained from the wavelet transform, giving us confidence in our implementation. For further details of the wavelet transform, we refer the reader to Soroldoni et al. (2014).

Acknowledgements

We thank O. Pourquié, A. Aulehla and A. Oates for critical discussion. Some images were taken at the Nikon Imaging Center at Harvard Medical School.

Competing interests

The authors declare no competing or financial interests.

Author contributions

Conceptualization: K.I., T.W.H., S.G.M.; Methodology: K.I., T.W.H., Z.M.C., D.W.K.S., K.L.; Software: T.W.H., D.L.R.; Formal analysis: T.W.H.; Investigation: K.I.; Writing - original draft: K.I., T.W.H., S.G.M.; Writing - review & editing: K.I., T.W.H., S.G.M.; Supervision: Y.B., T.M., S.G.M.; Project administration: S.G.M.; Funding acquisition: K.I., S.G.M.

Funding

The work was supported by the PRESTO program of the Japan Science and Technology Agency and a National Institutes of Health grant (R01GM107733). This work was partially supported by Grants-in-Aid for Scientific Research from the Ministry of Education, Culture, Sports, Science and Technology (MEXT), Japan (Y.B. and T.M.). T.W.H. was supported by a Herchel Smith Graduate Fellowship (University of Cambridge). K.I. acknowledges a Postdoctoral Fellowship for Research Abroad (Japan Society for the Promotion of Science). Deposited in PMC for release after 12 months.

Supplementary information

Supplementary information available online at <http://dev.biologists.org/lookup/doi/10.1242/dev.161257.supplemental>

References

- Akiyama, R., Masuda, M., Tsuge, S., Bessho, Y. and Matsui, T. (2014). An anterior limit of FGF/Erk signal activity marks the earliest future somite boundary in zebrafish. *Development* **141**, 1104-1109.
- Ares, S., Morelli, L. G., Jörg, D. J., Oates, A. C. and Julicher, F. (2012). Collective modes of coupled phase oscillators with delayed coupling. *Phys. Rev. Lett.* **108**, 204101.
- Ay, A., Holland, J., Sperlea, A., Devakanmalai, G. S., Knierer, S., Sangervasi, S., Stevenson, A. and Ozbudak, E. M. (2014). Spatial gradients of protein-level time delays set the pace of the traveling segmentation clock waves. *Development* **141**, 4158-4167.
- Bajard, L., Morelli, L. G., Ares, S., Pécraux, J., Julicher, F. and Oates, A. C. (2014). Wnt-regulated dynamics of positional information in zebrafish somitogenesis. *Development* **141**, 1381-1391.
- Baker, R. E., Schnell, S. and Maini, P. K. (2006). A clock and wavefront mechanism for somite formation. *Dev. Biol.* **293**, 116-126.
- Ben-Zvi, D. and Barkai, N. (2010). Scaling of morphogen gradients by an expansion-repression integral feedback control. *Proc. Natl. Acad. Sci. USA* **107**, 6924-6929.
- Cooke, J. (1975). Control of somite number during morphogenesis of a vertebrate, *Xenopus laevis*. *Nature* **254**, 196-199.
- Cooke, J. (1981). Scale of body pattern adjusts to available cell number in amphibian embryos. *Nature* **290**, 775-778.
- Cooke, J. and Zeeman, E. C. (1976). A clock and wavefront model for control of the number of repeated structures during animal morphogenesis. *J. Theor. Biol.* **58**, 455-476.
- Cotterell, J., Robert-Moreno, A. and Sharpe, J. (2015). A local, self-organizing reaction-diffusion model can explain somite patterning in embryos. *Cell Syst.* **1**, 257-269.
- Delaune, E. A., Francois, P., Shih, N. P. and Amacher, S. L. (2012). Single-cell-resolution imaging of the impact of Notch signaling and mitosis on segmentation clock dynamics. *Dev. Cell* **23**, 995-1005.
- Dequeant, M.-L., Glynn, E., Gaudenz, K., Wahl, M., Chen, J., Mushegian, A. and Pourquie, O. (2006). A complex oscillating network of signaling genes underlies the mouse segmentation clock. *Science* **314**, 1595-1598.
- Diez del Corral, R., Olivera-Martinez, I., Goriely, A., Gale, E., Maden, M. and Storey, K. (2003). Opposing FGF and retinoid pathways control ventral neural pattern, neuronal differentiation, and segmentation during body axis extension. *Neuron* **40**, 65-79.
- Dubrulle, J. and Pourquie, O. (2004). *fgf8* mRNA decay establishes a gradient that couples axial elongation to patterning in the vertebrate embryo. *Nature* **427**, 419-422.
- Dubrulle, J., McGrew, M. J. and Pourquie, O. (2001). FGF signaling controls somite boundary position and regulates segmentation clock control of spatiotemporal Hox gene activation. *Cell* **106**, 219-232.
- Elsdale, T., Pearson, M. and Whitehead, M. (1976). Abnormalities in somite segmentation following heat shock to *Xenopus* embryos. *J. Embryol. Exp. Morphol.* **35**, 625-635.
- Giudicelli, F., Ozbudak, E. M., Wright, G. J. and Lewis, J. (2007). Setting the tempo in development: an investigation of the zebrafish somite clock mechanism. *PLoS Biol.* **5**, e150.
- Gomez, C., Özbudak, E. M., Wunderlich, J., Baumann, D., Lewis, J. and Pourquie, O. (2008). Control of segment number in vertebrate embryos. *Nature* **454**, 335-339.
- Goudevenou, K., Martin, P., Yeh, Y.-J., Jones, P. and Sablitzky, F. (2011). *Def6* is required for convergent extension movements during zebrafish gastrulation downstream of Wnt5b signaling. *PLoS ONE* **6**, e26548.
- Gregor, T., Bialek, W., de Ruyter van Steveninck, R. R., Tank, D. W. and Wieschaus, E. F. (2005). Diffusion and scaling during early embryonic pattern formation. *Proc. Natl. Acad. Sci. USA* **102**, 18403-18407.
- Gregor, T., McGregor, A. P. and Wieschaus, E. F. (2008). Shape and function of the Bicoid morphogen gradient in dipteran species with different sized embryos. *Dev. Biol.* **316**, 350-358.

- Gunawardena, J.** (2014). Models in biology: 'accurate descriptions of our pathetic thinking'. *BMC Biol.* **12**, 29.
- Haines, L., Neyt, C., Gautier, P., Keenan, D. G., Bryson-Richardson, R. J., Holloway, G. E., Cole, N. J. and Currie, P. D.** (2004). Met and Hgf signaling controls hypaxial muscle and lateral line development in the zebrafish. *Development* **131**, 4857-4869.
- Harima, Y., Takashima, Y., Ueda, Y., Ohtsuka, T. and Kageyama, R.** (2012). Accelerating the tempo of the segmentation clock by reducing the number of introns in the *Hes7* gene. *Cell Rep.* **3**, 1-7.
- Herrgen, L., Ares, S., Morelli, L. G., Schröter, C., Julicher, F. and Oates, A. C.** (2010). Intercellular coupling regulates the period of the segmentation clock. *Curr. Biol.* **20**, 1244-1253.
- Holley, S. A., Geisler, R. and Nusslein-Volhard, C.** (2000). Control of *her1* expression during zebrafish somitogenesis by a delta-dependent oscillator and an independent wave-front activity. *Genes Dev.* **14**, 1678-1690.
- Howard, M. and ten Wolde, P. R.** (2005). Finding the center reliably: robust patterns of developmental gene expression. *Phys. Rev. Lett.* **95**, 208103.
- Hubaud, A. and Pourquie, O.** (2014). Signalling dynamics in vertebrate segmentation. *Nat. Rev. Mol. Cell Biol.* **15**, 709-721.
- Inomata, H., Shibata, T., Haraguchi, T. and Sasai, Y.** (2013). Scaling of dorsal-ventral patterning by embryo size-dependent degradation of Spemann's organizer signals. *Cell* **153**, 1296-1311.
- Jörg, D. J., Morelli, L. G., Soroldoni, D., Oates, A. C. and Julicher, F.** (2015). Continuum theory of gene expression waves during vertebrate segmentation. *New J. Phys.* **17**, 093042.
- Jörg, D. J., Oates, A. C. and Julicher, F.** (2016). Sequential pattern formation governed by signaling gradients. *Phys. Biol.* **13**, 05LT03.
- Kawanishi, T., Kaneko, T., Moriyama, Y., Kinoshita, M., Yokoi, H., Suzuki, T., Shimada, A. and Takeda, H.** (2013). Modular development of the teleost trunk along the dorsoventral axis and *zic1/zic4* as selector genes in the dorsal module. *Development* **140**, 1486-1496.
- Kim, W., Matsui, T., Yamao, M., Ishibashi, M., Tamada, K., Takumi, T., Kohno, K., Oba, S., Ishii, S., Sakumura, Y. et al.** (2011). The period of the somite segmentation clock is sensitive to Notch activity. *Mol. Biol. Cell* **22**, 3541-3549.
- Komatsu, N., Aoki, K., Yamada, M., Yukinaga, H., Fujita, Y., Kamioka, Y. and Matsuda, M.** (2011). Development of an optimized backbone of FRET biosensors for kinases and GTPases. *Mol. Biol. Cell* **22**, 4647-4656.
- Krol, A. J., Roellig, D., Dequeant, M.-L., Tassy, O., Glynn, E., Hattem, G., Mushagian, A., Oates, A. C. and Pourquie, O.** (2011). Evolutionary plasticity of segmentation clock networks. *Development* **138**, 2783-2792.
- Lander, A. D., Nie, Q., Vargas, B. and Wan, F. Y.** (2011). Size-normalized Robustness of Dpp Gradient in Drosophila Wing Imaginal Disc. *J. Mech. Mater. Struct.* **6**, 321-350.
- Lauschke, V. M., Tsiarris, C. D., François, P. and Aulehla, A.** (2013). Scaling of embryonic patterning based on phase-gradient encoding. *Nature* **493**, 101-105.
- Masamizu, Y., Ohtsuka, T., Takashima, Y., Nagahara, H., Takenaka, Y., Yoshikawa, K., Okamura, H. and Kageyama, R.** (2006). Real-time imaging of the somite segmentation clock: revelation of unstable oscillators in the individual presomitic mesoderm cells. *Proc. Natl. Acad. Sci. USA* **103**, 1313-1318.
- McHale, P., Rappel, W.-J. and Levine, H.** (2006). Embryonic pattern scaling achieved by oppositely directed morphogen gradients. *Phys. Biol.* **3**, 107-120.
- Megason, S. G.** (2009). In toto imaging of embryogenesis with confocal time-lapse microscopy. *Methods Mol. Biol.* **546**, 317-332.
- Morelli, L. G., Ares, S., Herrgen, L., Schröter, C., Jülicher, F. and Oates, A. C.** (2009). Delayed coupling theory of vertebrate segmentation. *HFSP J.* **3**, 55-66.
- Nikaido, M., Tada, M., Saji, T. and Ueno, N.** (1997). Conservation of BMP signaling in zebrafish mesoderm patterning. *Mech. Dev.* **61**, 75-88.
- O'Connor, M. B., Umulis, D., Othmer, H. G. and Blair, S. S.** (2006). Shaping BMP morphogen gradients in the Drosophila embryo and pupal wing. *Development* **133**, 183-193.
- Olivera-Martinez, I. and Storey, K. G.** (2007). Wnt signals provide a timing mechanism for the FGF-retinoid differentiation switch during vertebrate body axis extension. *Development* **134**, 2125-2135.
- Ozbudak, E. M. and Lewis, J.** (2008). Notch signalling synchronizes the zebrafish segmentation clock but is not needed to create somite boundaries. *PLoS Genet.* **4**, e15.
- Palmeirim, I., Henrique, D., Ish-Horowicz, D. and Pourquie, O.** (1997). Avian hairy gene expression identifies a molecular clock linked to vertebrate segmentation and somitogenesis. *Cell* **91**, 639-648.
- Primmitt, D. R., Stern, C. D. and Keynes, R. J.** (1988). Heat shock causes repeated segmental anomalies in the chick embryo. *Development* **104**, 331-339.
- Primmitt, D. R., Norris, W. E., Carlson, G. J., Keynes, R. J. and Stern, C. D.** (1989). Periodic segmental anomalies induced by heat shock in the chick embryo are associated with the cell cycle. *Development* **105**, 119-130.
- Rauch, G. J., Hammerschmidt, M., Blader, P., Schuerte, H. E., Strahle, U., Ingham, P. W., McMahon, A. P. and Haffter, P.** (1997). *Wnt5* is required for tail formation in the zebrafish embryo. *Cold Spring Harb. Symp. Quant. Biol.* **62**, 227-234.
- Roy, M. N., Prince, V. E. and Ho, R. K.** (1999). Heat shock produces periodic somitic disturbances in the zebrafish embryo. *Mech. Dev.* **85**, 27-34.
- Saga, Y.** (2012). The synchrony and cyclicity of developmental events. *Cold Spring Harb. Perspect. Biol.* **4**, a008201.
- Sari, D. W. K., Akiyama, R., Naoki, H., Ishijima, H., Bessho, Y. and Matsui, T.** (2018). Time-lapse observation of stepwise regression of Erk activity in zebrafish presomitic mesoderm. *Sci. Rep.* **8**, 4335.
- Sawada, A., Shinya, M., Jiang, Y. J., Kawakami, A., Kuroiwa, A. and Takeda, H.** (2001). Fgf/MAPK signalling is a crucial positional cue in somite boundary formation. *Development* **128**, 4873-4880.
- Schindelin, J., Arganda-Carreras, I., Frise, E., Kaynig, V., Longair, M., Pietzsch, T., Preibisch, S., Rueden, C., Saalfeld, S., Schmid, B. et al.** (2012). Fiji: an open-source platform for biological-image analysis. *Nat. Methods* **9**, 676-682.
- Schröter, C. and Oates, A. C.** (2010). Segment number and axial identity in a segmentation clock period mutant. *Curr. Biol.* **20**, 1254-1258.
- Schröter, C., Herrgen, L., Cardona, A., Brouhard, G. J., Feldman, B. and Oates, A. C.** (2008). Dynamics of zebrafish somitogenesis. *Dev. Dyn.* **237**, 545-553.
- Shih, N. P., Francois, P., Delaune, E. A. and Amacher, S. L.** (2015). Dynamics of the slowing segmentation clock reveal alternating two-segment periodicity. *Development* **142**, 1785-1793.
- Soroldoni, D., Jorg, D. J., Morelli, L. G., Richmond, D. L., Schindelin, J., Julicher, F. and Oates, A. C.** (2014). Genetic oscillations. A Doppler effect in embryonic pattern formation. *Science* **345**, 222-225.
- Soza-Ried, C., Ozturk, E., Ish-Horowicz, D. and Lewis, J.** (2014). Pulses of Notch activation synchronise oscillating somite cells and entrain the zebrafish segmentation clock. *Development* **141**, 1780-1788.
- Steventon, B., Duarte, F., Lagadec, R., Mazan, S., Nicolas, J. F. and Hirsinger, E.** (2016). Species-specific contribution of volumetric growth and tissue convergence to posterior body elongation in vertebrates. *Development* **143**, 1732-1741.
- Stulberg, M. J., Lin, A., Zhao, H. and Holley, S. A.** (2012). Crosstalk between Fgf and Wnt signaling in the zebrafish tailbud. *Dev. Biol.* **369**, 298-307.
- Takahashi, J., Ohbayashi, A., Oginuma, M., Saito, D., Mochizuki, A., Saga, Y. and Takada, S.** (2010). Analysis of Ripply1/2-deficient mouse embryos reveals a mechanism underlying the rostro-caudal patterning within a somite. *Dev. Biol.* **342**, 134-145.
- Thorpe, C. J., Weidinger, G. and Moon, R. T.** (2005). Wnt/beta-catenin regulation of the Sp1-related transcription factor *sp51* promotes tail development in zebrafish. *Development* **132**, 1763-1772.
- Tsiarris, C. D. and Aulehla, A.** (2016). Self-Organization of Embryonic Genetic Oscillators into Spatiotemporal Wave Patterns. *Cell* **164**, 656-667.
- Umulis, D. M. and Othmer, H. G.** (2013). Mechanisms of scaling in pattern formation. *Development* **140**, 4830-4843.
- Uriu, K., Morishita, Y. and Iwasa, Y.** (2009). Traveling wave formation in vertebrate segmentation. *J. Theor. Biol.* **257**, 385-396.
- Wahl, M. B., Deng, C., Lewandoski, M. and Pourquie, O.** (2007). FGF signaling acts upstream of the NOTCH and WNT signaling pathways to control segmentation clock oscillations in mouse somitogenesis. *Development* **134**, 4033-4041.
- Westerfield, M.** (2000). *The Zebrafish Book. A Guide for the Laboratory Use of Zebrafish (Danio rerio)*. Eugene: University of Oregon Press.

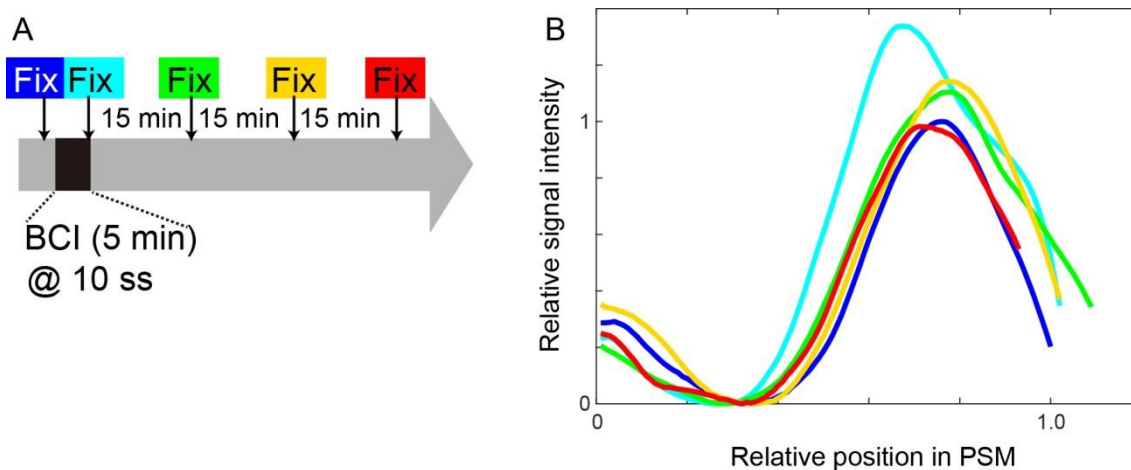


Fig. S1 Time course analysis of dpErk intensity before and after transient BCI treatment. (A) Schematic illustration of the experiment. At each time point, control and treated embryos (seven embryos each) were fixed and analyzed. **(B)** Intensity curves were calculated by averaging intensity curves of treated embryos. Relative signal intensity (y axis) was determined by scaling factors: (maximum intensity of treated embryos) / (maximum intensity of control embryos at the corresponding time points). Relative position (x axis) was determined by normalizing positions in PSM in treated embryos by averaged PSM length of control embryos at the corresponding time points. Colors correspond to the colors in (A). dpErk intensity increases immediately after BCI treatment, and comes back to normal after 15 min of wash.

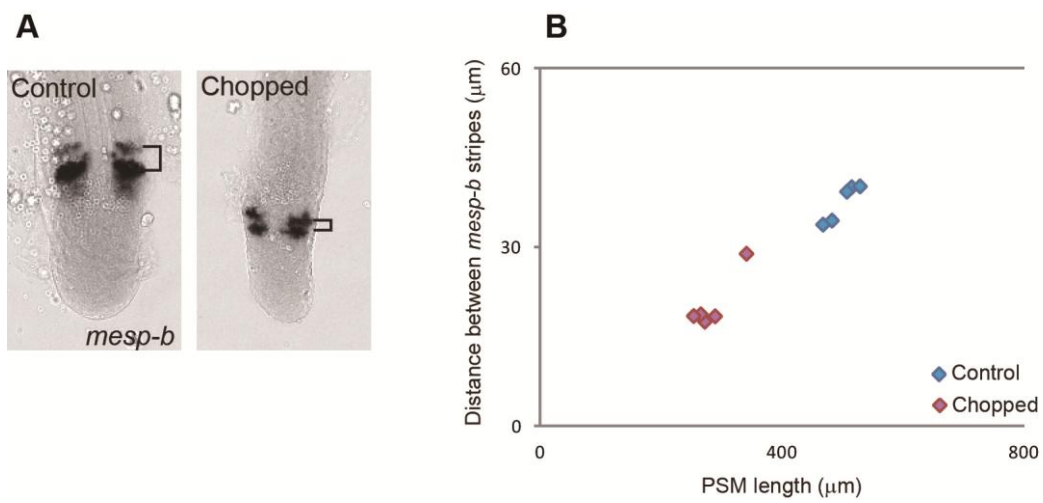


Fig. S2 Scaling of *mesp-b* stripe. (A) *in situ* hybridization samples of *mesp-b*. (B) PSM length vs distance between *mesp-b* stripes.

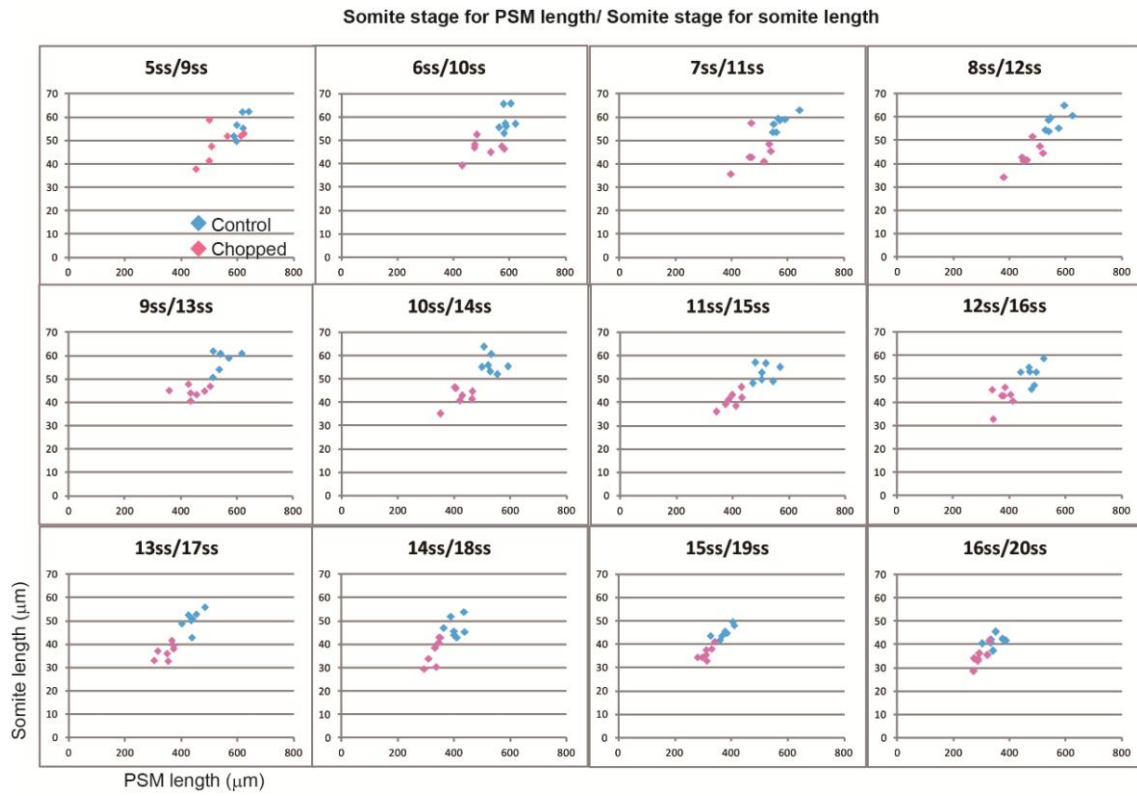


Fig. S3 Somite size vs PSM size between control and chopped embryos from different somite stages.

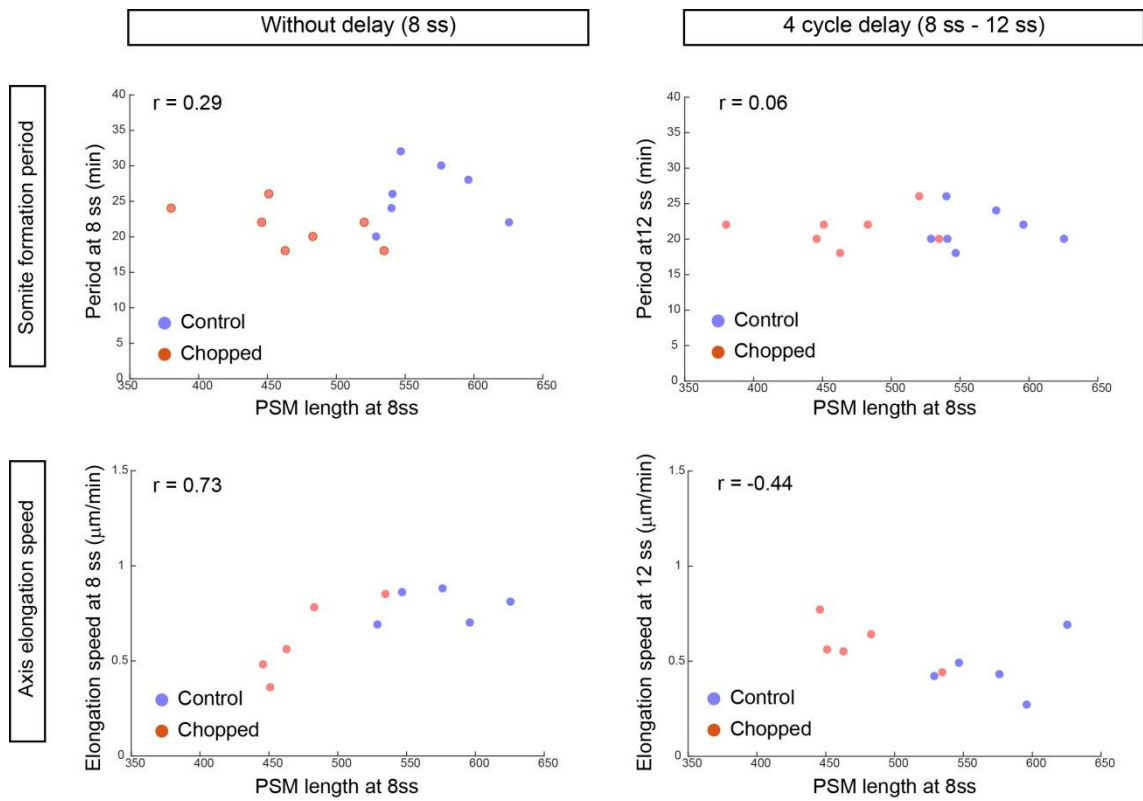


Fig. S4 Clock period and axis elongation speed with and without 4 cycle delay. Neither clock period nor axis elongation speed scale with PSM length even when the time delay is taken into consideration.

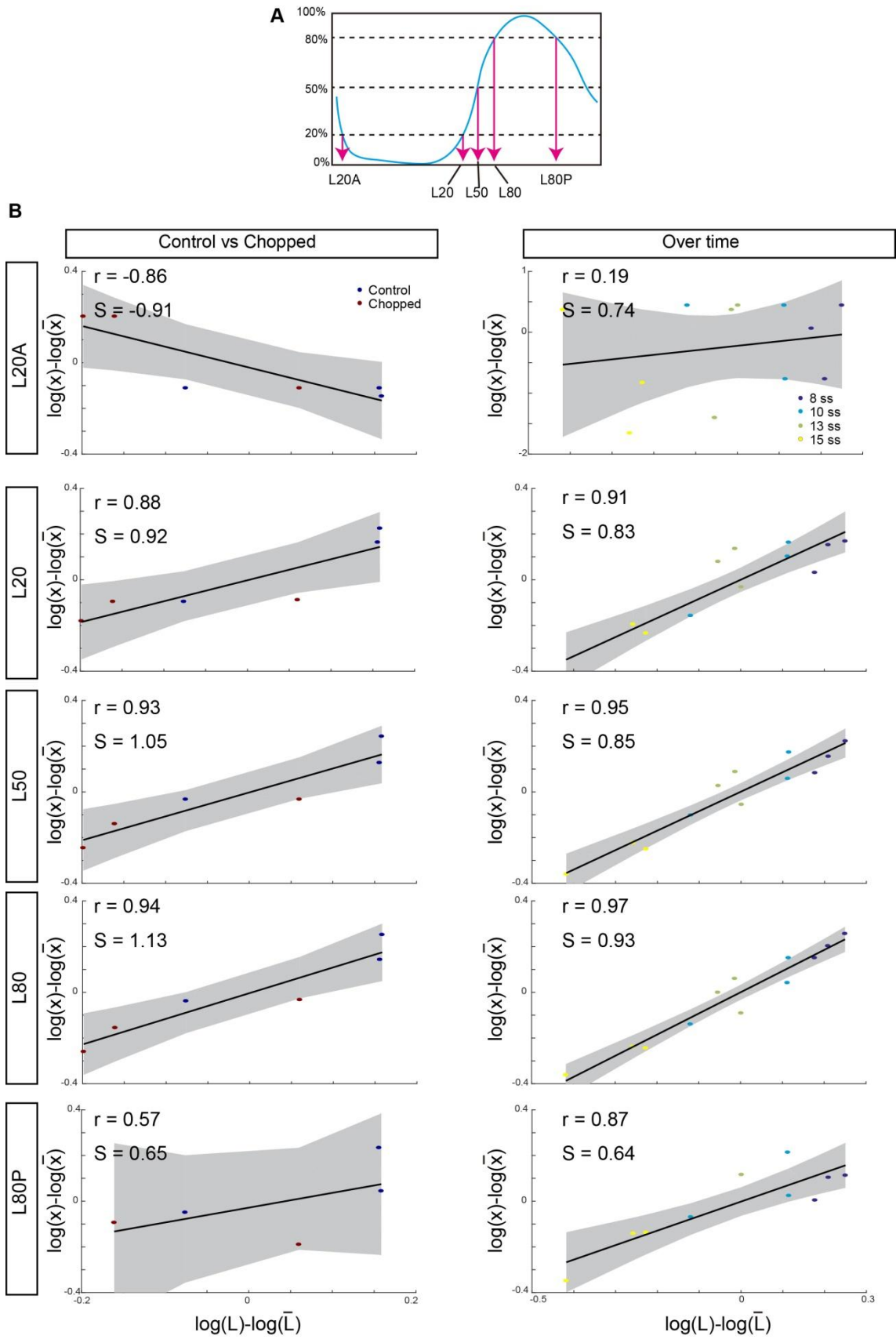


Fig. S5 dpErk scaling for different thresholds. (A) Schematic illustration of position names. (B) For each PSM, log-deviation in the position $\log(x/\bar{x}) = \log(x) - \log(\bar{x})$ is plotted against log-deviation in the PSM length $\log(L/\bar{L}) = \log(L) - \log(\bar{L})$, for different dpErk threshold intensities. The scaling coefficient S is obtained by linear regression (95% confidence interval on the slope is shown in gray). Correlation r is shown. In both cases (control vs chopped, and over time), L20, L50 and L80 scales with PSM length more than other positions. For detail, see (Hamaratoglu et al., 2011).

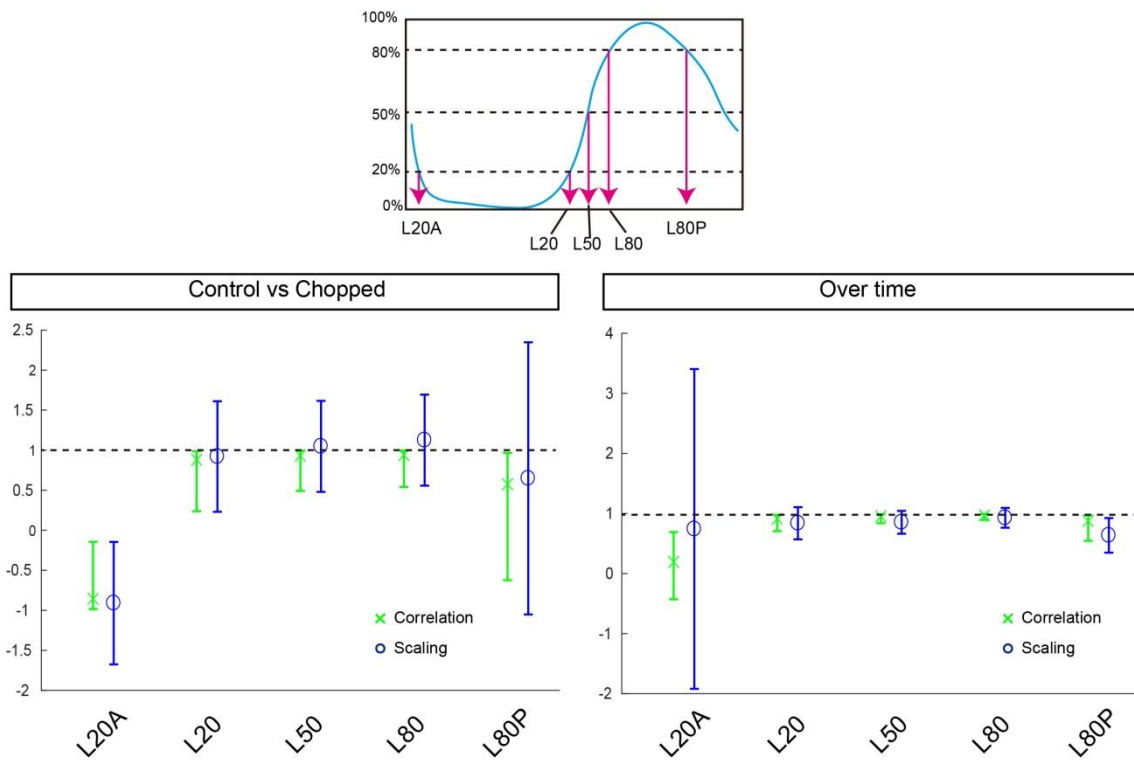


Fig. S6 Correlation coefficient and scaling coefficient for dpErk gradient. dpErk correlation (x) and scaling (o) for several gradient positions. Error bars represent the 95% confidence intervals. At L20, L50 and L80, the correlation and scaling coefficients are closer to 1, compared to other positions, which is consistent with Fig. S5. For detail, see (Hamaratoglu et al., 2011).

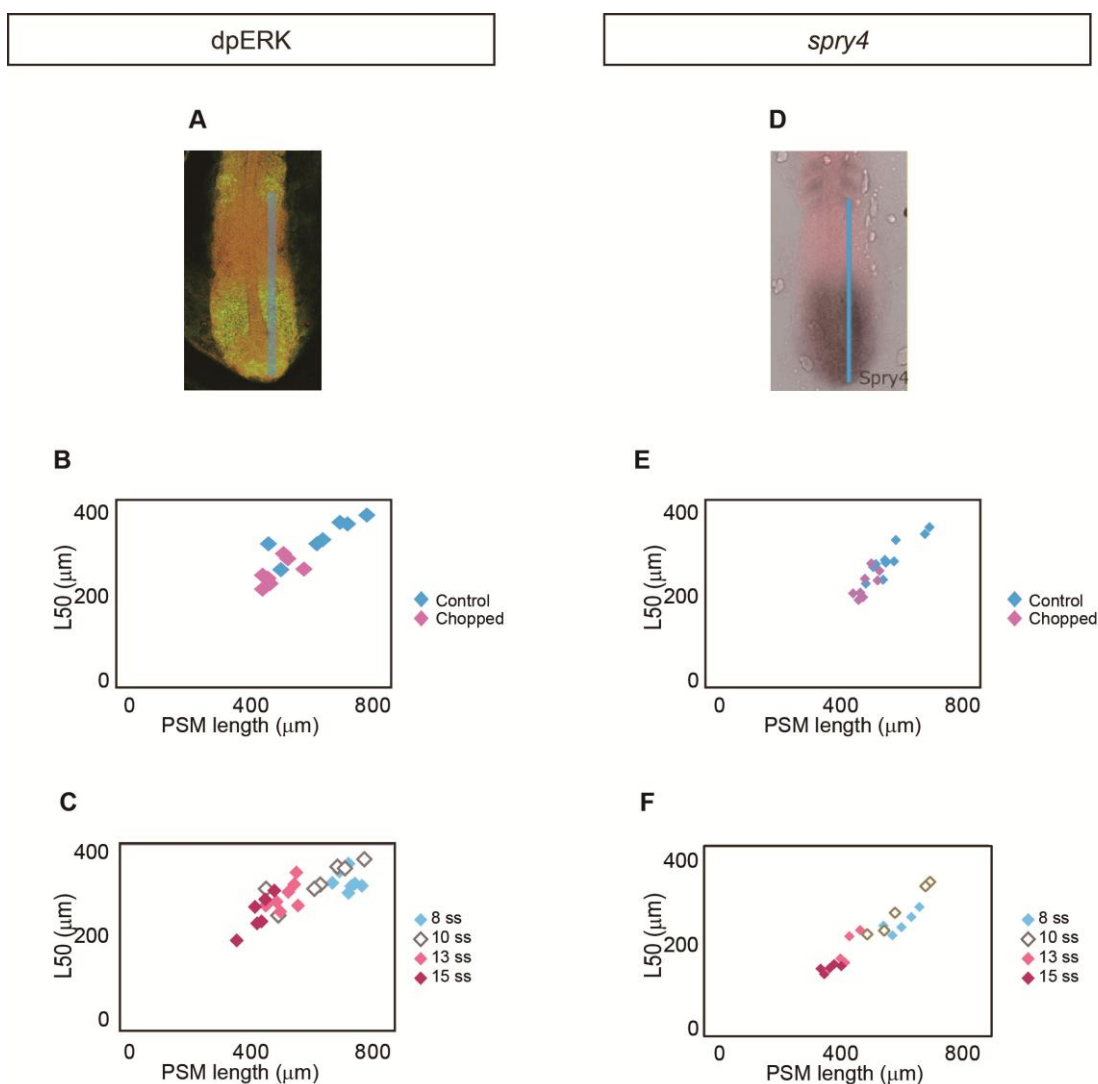


Fig. S7 Fgf activity scaling detected by dpErk and *spry4*. (A to C) L50 analysis on dpErk. (D to F) L50 analysis on *spry4* expression. (A) dpErk activity was detected by immunostaining. (D) *spry4* mRNA was detected by in situ hybridization. (B and C, E and F) L50 was calculated using *spry4* in situ hybridization samples similarly as in Fig. 3I. For both dpErk and *spry4*, L50 was found to scale with PSM length both between control and chopped embryos (B and E) and over time (C and F)

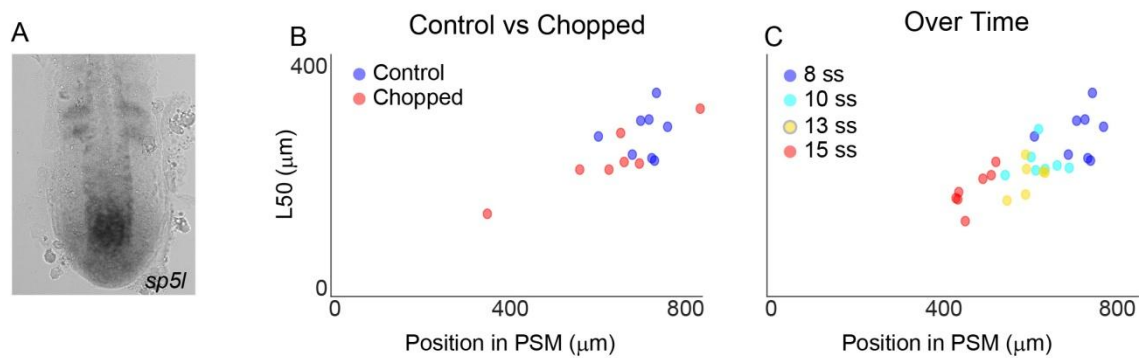


Fig. S8 Wnt signal scales with PSM length. (A) *sp5l* mRNA was detected by in situ hybridization. (B and C) L50 was calculated using *sp5l* in situ hybridization samples similarly as in Fig. 3P. L50 was found to scale with PSM length both between control and chopped embryos (B) and over time (C)

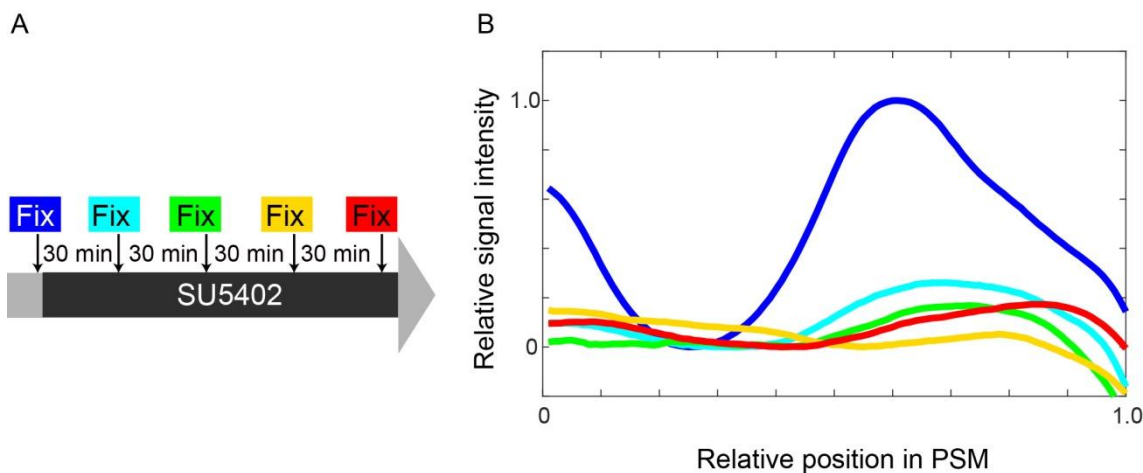


Fig. S9 Fgf activity gradient following SU5402 treatment (A) Schematic illustration of the experiment. At each time point, control and treated embryos (seven embryos each) were fixed and analyzed. (B) Intensity curves were calculated by averaging intensity curves of treated embryos. Relative signal intensity (y axis) was determined by using scaling factors: (maximum intensity of treated embryos) / (maximum intensity of control embryos at the corresponding time points). Relative position (x axis) was determined by normalizing positions in the PSM in treated embryos by averaged PSM length of control embryos at the corresponding time points. Colors correspond to the colors in (A). dpErk intensity drops immediately after onset of SU5402 treatment, and remains almost the same level over the course of experiment. Somites were still formed with relatively flat gradient of dpErk (Fig. 4L and M), possibly suggesting that dpErk is not the direct readout of the wavefront activity (see also discussion in the main text).

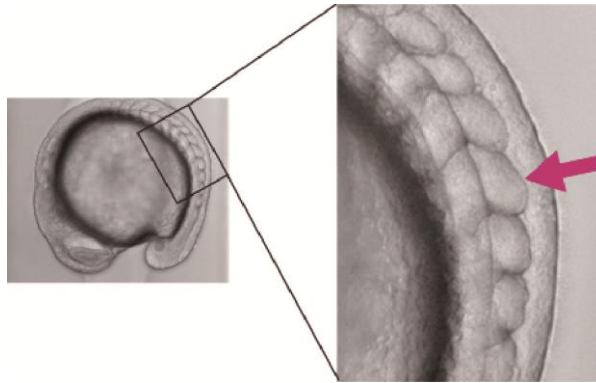


Fig. S10 Long-term SU5402 treatment under constant dark condition The embryos were treated with SU5402 at low concentration ($16\mu\text{M}$) for 4 hrs with the light completely blocked. One or two larger somites were formed (magenta arrow in the right panel) several cycles after initiation of the treatment (10 out of 11).

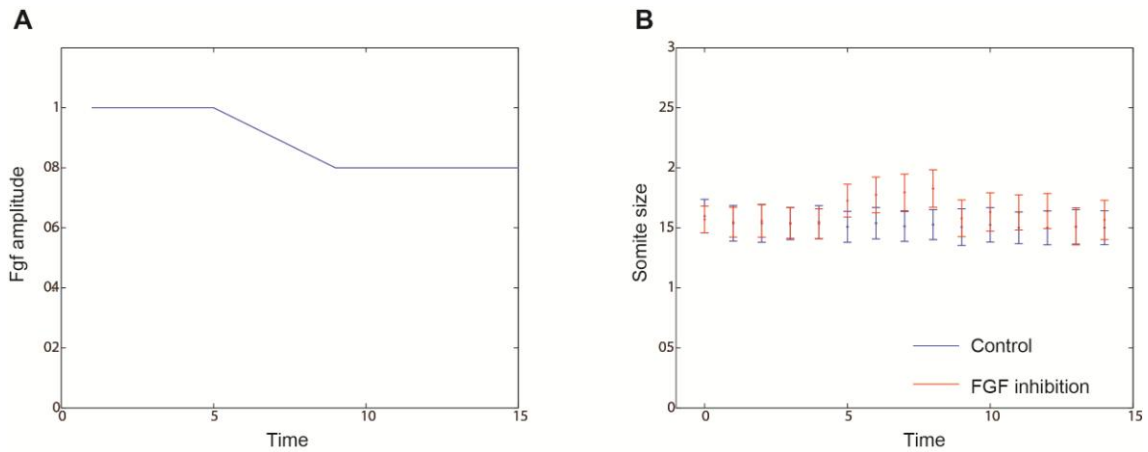


Fig. S11 Increasing Fgf inhibition can cause multiple larger somites. Here using the clock and scaled gradient model, we simulated the situation in which Fgf inhibition occurs increasingly, rather than in a step-wise manner (A). (B) As a result, multiple larger somites were predicted to be formed, consistent with the result in chick (Cotterell et al., 2015). Error bars denote s.d.

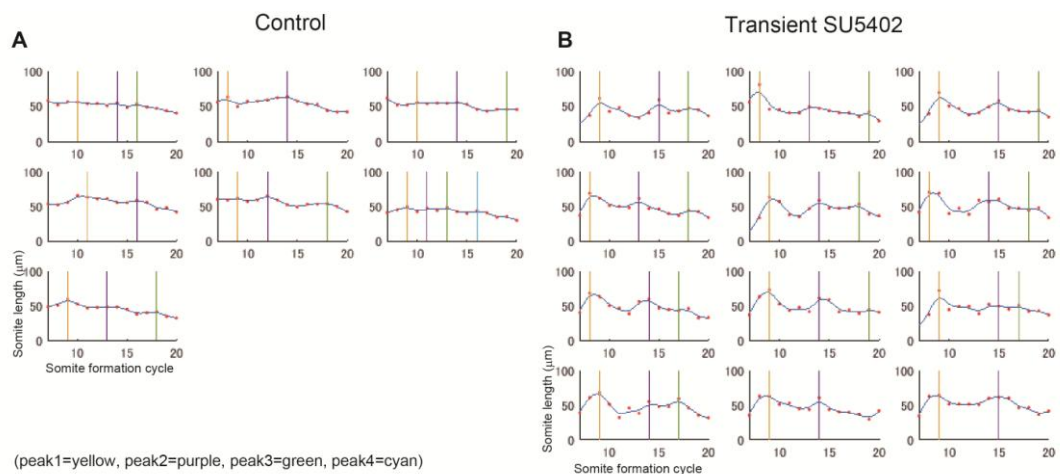


Fig. S12 Somite length change in individual samples. Somite sizes were measured using time-lapse imaging both in control (**A**) and SU5402 treated embryos (**B**). The peaks are detected using matlab function. Note the periodic change in somite length is much more obvious in SU5402 treated embryos, compared to control embryos.

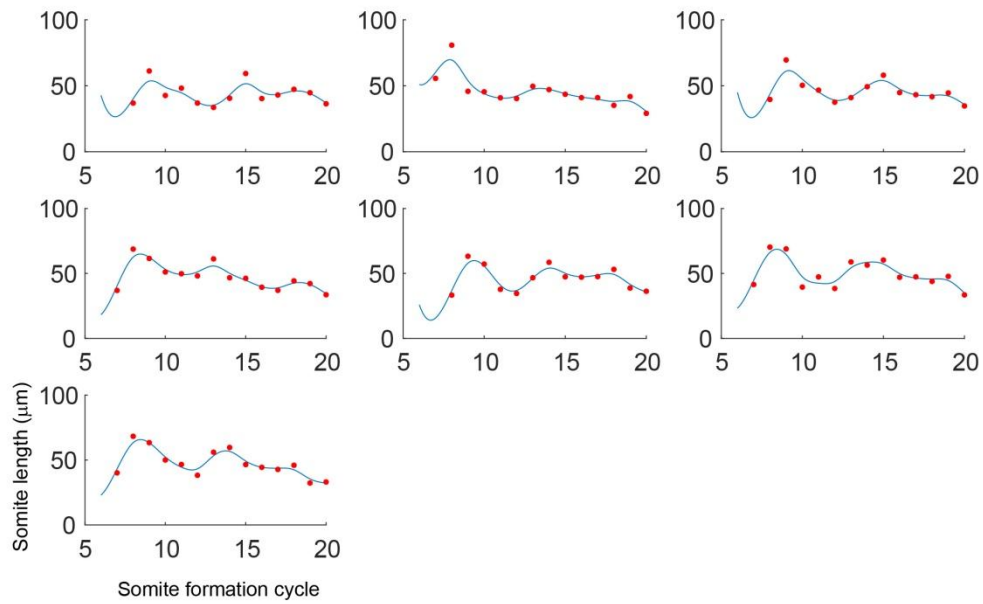


Fig. S13 Somite length change in individual samples in long-term SU5402 treatment. Somite sizes were measured using time-lapse imaging. As predicted in the simulation of the clock and scaled gradient model (Fig. 4K), the echo effect was observed.

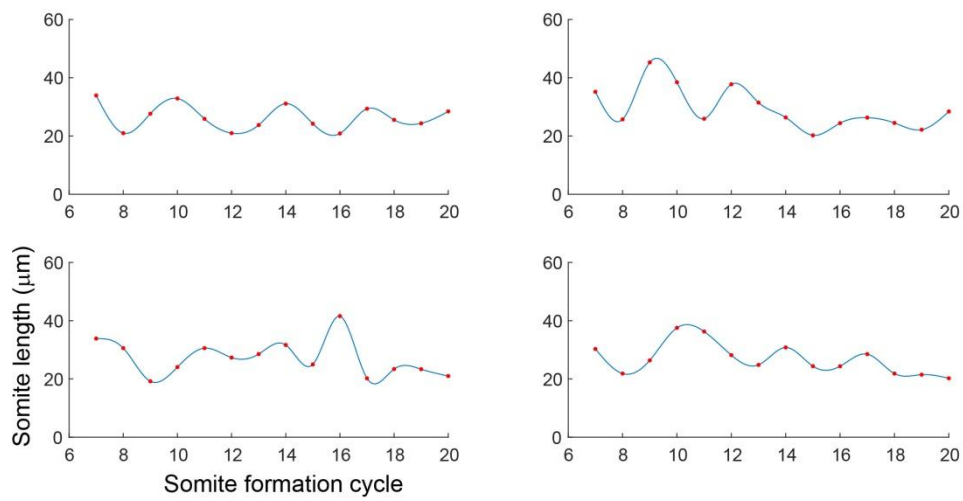


Fig. S14 Somite length change in individual samples in short-term BCI treatment. Somite sizes were measured using time-lapse imaging. Similar to SU5402 treatment, the echo effect was observed.

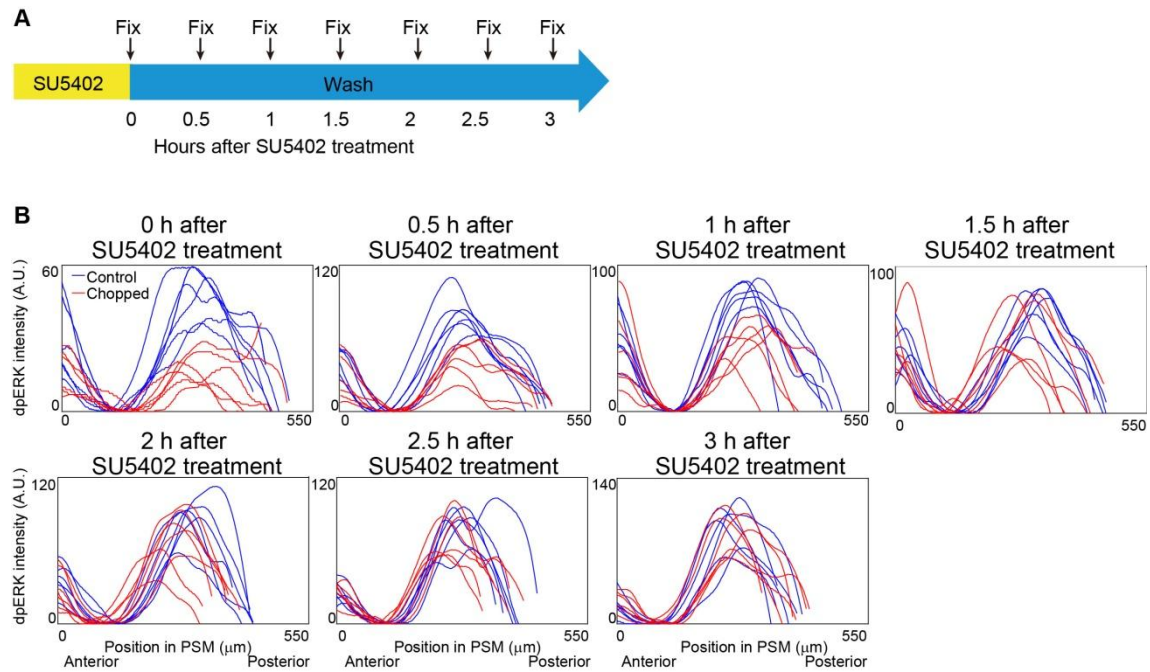


Fig. S15 dpErk intensity change in individual samples for echo experiment. (A) Schematic illustration of the experiment. Samples were fixed every 30 min after SU5402 treatment. (B) Intensity profiles of dpErk immunostaining for control (blue) and treated embryos (red).

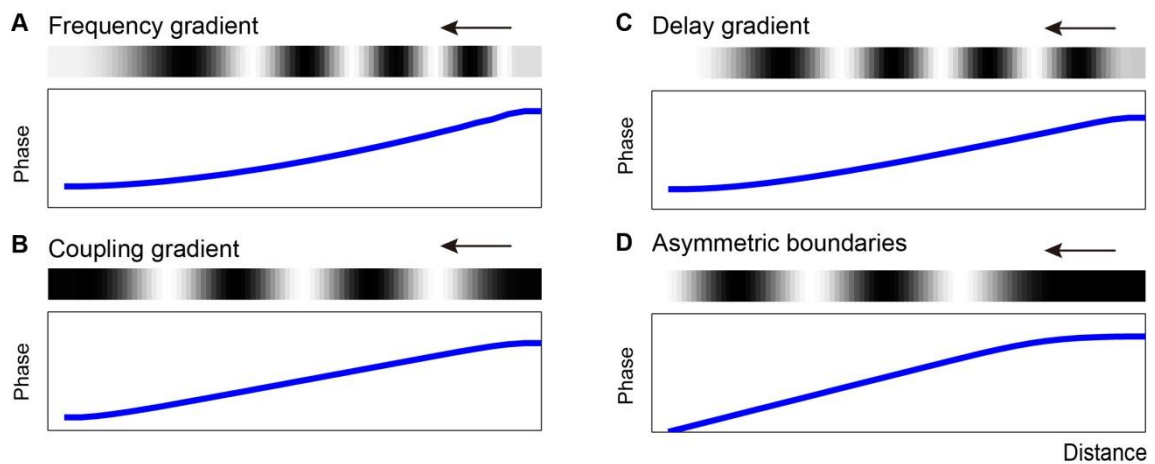


Fig. S16 Traveling wavevcs arise under many conditions. Simulation of the Kuramoto model (see supplementary materials and methods for detail) with reflective boundary conditions and linear gradients in frequency (A), coupling strength (B), or phase delay (C) generate phase gradients and hence traveling waves. This is also observed in the absence of any gradients, but with a cut boundary at the anterior (D).



Movie 1 Simulation of clock and scaled gradient model

In the clock and scaled gradient model, each cell has a clock and a morphogen that shows a gradient in posterior to anterior direction. For simplicity, we assumed the clock oscillates synchronously along the PSM (blue in upper column) but phase gradients do not affect the results of the model. The morphogen gradient always scales with PSM size by an unspecified mechanism (red in lower column).. The mature somites are indicated by black lines, whereas 4 somites that are not visible but already determined are indicated by gray lines.

Supplementary Materials and Methods

Formulation of the Clock and Scaled Gradient model

As outlined in the main text, we develop a simple model of somitogenesis based on two key features: a ‘clock’ and a ‘scaled gradient’. Note, we do not assign molecular identities to either the clock or the gradient, although, as described in the main text, we have candidates for each. To formulate the model mathematically, we convert our observations of the system into a set of concrete mathematical assumptions, namely:

1. **Clock:** To model an oscillator, we describe its phase by:

$$\frac{\partial \phi}{\partial t} = \frac{2\pi}{T} \quad (\text{S1})$$

where T is the clock period. Here we assume that the clock oscillates synchronously throughout the PSM (see below for the more general case where ϕ also varies in space).

2. **Gradient** We model the gradient, $g(x)$, by the function:

$$g(x) = g_0 G(x/l_{\text{PSM}}) \quad (\text{S2})$$

where x is the distance to the tailbud, and l_{PSM} is the length of the PSM (from tailbud to mature somite boundary). The functional form $G(x/l_{\text{PSM}})$ embodies the scaling of the gradient with PSM size, with the parameter g_0 denoting the overall gradient amplitude. We choose G to be of the form: $G(u) = 1 + \tanh(\beta(0.5 - u))$, with $\beta = 3$, a gradient chosen to qualitatively reflect the dpErk gradient from Fig. 3 in the main text. For completeness, we also include noise in the gradient by adding a random number at each position, normally distributed with standard deviation σ . However, we emphasize that we see similar qualitative somitogenesis dynamics regardless of the precise functional form of G - even a simple linear gradient ($G(u) = 1 - u$) can recapitulate the *in vivo* behaviour rather closely (Fig. 4).

3. **Somite determination** We assume that a somite boundary is placed when the clock reaches a certain value (we take $\text{mod}(\phi, 2\pi) = 0$) and at the position where the gradient exceeds a certain threshold, α i.e. the i^{th} somite boundary position, b_i , is given by $g(t_i - b_i) = \alpha$, where t_i is the position of the tail at this timepoint (and thus $t_i - b_i$ is the distance from b_i to the tail). We must also include the 4-cycle delay as outlined in Fig. 4A - when the i^{th} somite boundary is specified, b_i , it takes a further 4 cycles (i.e. 8π phase) for it to fully mature.
4. **Changes in PSM size.** We assume that PSM size reduces as somites mature at the anterior end. We also incorporate tail elongation to increase PSM size. For the time-window we are studying, our data suggests that tail elongation speed is approximately constant; therefore we set it to be a constant value, v .
5. **Initial conditions** The key initial condition we must set is the initial PSM size, which we label as $l_{\text{PSM}}^{(0)}$.
6. **First four somites** In the above, we have assumed (i) the PSM size is defined from tailbud to mature somite boundary and (ii) somites take 4 cycles to fully form. These assumptions break down for the earliest somites, which form (i) at a faster rate than the rest, (ii) before the tailbud has formed and gastrulation is occurring, and (iii) before there is a clear ‘mature somite’ boundary to set the PSM size in our model. Due to this complexity (and the fact that our data does not cover the earliest somites), we do not consider the first 4 cycles explicitly. Instead, we set the widths of the first 4 somites as equal to some arbitrary constant, l_{initial} , which is chosen such that somite size changes continuously from the 4th to the 5th somite.

Together, these assumptions form the basis for our model. The model is simple, containing only 4 free parameters $\{T, g_0, \alpha, v\}$ (and during unperturbed development, we can nondimensionalize the equations leaving only a **single free parameter**, α), as well as the initial conditions. The model’s simplicity allows us to obtain simple, qualitative insights into the phenomena and thus build an intuition for how somite sizes are controlled.

Model Results

Analytical solution

As per Fig. 4A, we write the position of somite boundary i as it is specified as b_i , and the tailbud position at this time as t_i . Without loss of generality (WLOG), the threshold condition $\alpha = g_0 G(x_i/l_{\text{PSM}})$ can be rewritten as $x_i/l_{\text{PSM}} = (1 - f)$ where f is the fraction along the PSM at which the boundary is placed. Then, the Clock and Scaled Gradient model gives:

$$b_i = f(t_i - b_{i-4}) + b_{i-4} \quad (\text{S3})$$

$$b_{i+1} = f(t_{i+1} - b_{i-3}) + b_{i-3} \quad (\text{S4})$$

Subtracting gives an expression for the newly specified somite size $l_i \equiv b_{i+1} - b_i$:

$$l_i = f v T + (1 - f) l_{i-4} \quad (\text{S5})$$

where we have used $t_{i+1} - t_i = vT$ due to tail elongation. For the steady state, we have $l_i = l_{i-4}$ and thus:

$$l = vT \quad (\text{S6})$$

i.e. we predict that somite size increases with clock period, and with tail speed and, at steady state, is independent of the specifics of the gradient (see Fig. 4C-F).

Now, if instead we set $v = 0$, then somites still form, according to:

$$l_i = (1 - f) l_{i-4} \quad (\text{S7})$$

i.e. there is a perfect geometric progression of somite sizes, as seen in an *in vitro* model of somitogenesis in which there is no tail elongation (see Fig. 4J)(Lauschke et al., 2013).

To consider the effects of perturbing the gradient, we allow steady state to be reached (i.e. $l_j \equiv b_{j+1} - b_j = vT$ for $j < i$), and then perturb f . Firstly, we consider the case outlined in Fig. 6 in which the gradient is perturbed transiently for a single cycle. Here we have:

$$b_i = f(t_i - b_{i-4}) + b_{i-4} \quad (\text{S8})$$

$$b_{i+1} = (f - \Delta f)(t_{i+1} - b_{i-3}) + b_{i-3} \quad (\text{S9})$$

$$b_{i+2} = f(t_{i+2} - b_{i-2}) + b_{i-2} \quad (\text{S10})$$

Computing $l_i \equiv b_{i+1} - b_i$ gives:

$$l_i = vT + \Delta f l_{\text{PSM}}^{(i)} \quad (\text{S11})$$

i.e. the i^{th} somite is larger. However, if we now examine the $(i + 1)^{\text{th}}$ somite, we find:

$$l_{i+1} = vT - \Delta f l_{\text{PSM}}^{(i+1)} \quad (\text{S12})$$

i.e. that the $(i + 1)^{\text{th}}$ somite is smaller. Furthermore, considering the fundamental 4-cycle periodicity of the equations, we predict (and show through simulation Fig. 6C) that this pattern of big somite followed by small somite is repeated every 4 cycles.

Secondly, we consider the case shown in Fig. 4 K-M, in which Fgf is continuously perturbed. Now we have:

$$b_i = f(t_i - b_{i-4}) + b_{i-4} \quad (\text{S13})$$

$$b_{i+1} = (f + \Delta f)(t_{i+1} - b_{i-3}) + b_{i-3} \quad (\text{S14})$$

$$b_{i+2} = (f + \Delta f)(t_{i+2} - b_{i-2}) + b_{i-2} \quad (\text{S15})$$

and so on. In this case, computing $l_i \equiv b_{i+1} - b_i$ gives:

$$l_i = vT + \Delta f l_{\text{PSM}}^{(i)} \quad (\text{S16})$$

i.e. this somite is altered in size. However, when we compute the size of the subsequent somites, e.g. $l_{i+1} \equiv b_{i+2} - b_{i+1}$

$$l_{i+1} = vT \quad (\text{S17})$$

we find that they return to their unperturbed value, exactly as seen *in vivo* (see Fig. 4L and M)*.

*Note also that our model predicts small somite size changes with 4-cycle periodicity (Fig. 4K), which was seen in Fig. S13

Simulations

We implement the equations described above using a custom MATLAB script[†]. To generate the figures in the main text, we used the parameters: $\{v = 1.5, \alpha = 1, g_0 = 1, T = 1\}$ and the initial conditions $\{l_{\text{initial}} = 2.9, l_{\text{PSM}}^{(0)} = 20\}$. For the chopped embryos we used the same parameters, but different initial conditions $\{l_{\text{initial}} = 0.7, l_{\text{PSM}}^{(0)} = 5\}$. For Fig. 4 C-F, we added noise to the gradient ($\sigma = 0.01$) and noise in the PSM measurement (i.e. normally distributed scatter with $\sigma_{\text{measure}} = 0.3$) to reflect the data in Fig. 1 and 2.

For the perturbations, we used the same parameters as wildtype but without noise (to more easily visualize differences between conditions) and:

- For transient Fgf activation (Fig. 4I), we set $g_0 = 1.1$ for the 10th cycle
- For sustained Fgf inhibition (Fig. 4I), we set $g_0 = 0.8$ for all times after the 9th cycle
- For the Fgf bead (Fig. 4I), we add a localized increase in the gradient, $g_{\text{bead}} \exp \left[- \left(\frac{x - x_{\text{bead}}}{w_{\text{bead}}} \right)^2 \right]$, with $g_{\text{bead}} = 0.5, x_{\text{bead}} = 29, w_{\text{bead}} = 2$.
- For the slower clock (Fig. 4I), we set $T = 2$.
- For the slower tail (Fig. 4I), we set $v = 1$.
- For sustained Fgf inhibition for Fig. 4K, we set $\sigma = 0.02$, and $g = 0.9$ for all times after the 24th cycle (which we relabel as the 0th cycle on the plot)
- For no axis elongation (Fig. 4J), we set $v = 0$.
- For Fig. 6C, we set $g_0 = 0.92$ for the 10th cycle, and plot the mean and standard deviation for 10 independent simulations with noise $\sigma = 0.03$, parameters chosen to reflect the *in vivo* data.
- For Fig. 6B, we repeated the above but with $g_0 = 0.85$ and no noise term to emphasize the effect for visualization purposes.
- For Fig. 6L-N, we used a higher number of repeats (1000 instead of 10) and a smaller noise ($\sigma = 0.02$) to better compare to the other models.

[†]<https://wiki.med.harvard.edu/SysBio/Megason/MegasonSoftware>

Origin of *her1* travelling waves

In this study, we found that the wavelength of *her1* waves does not play a central role in determining somite size. Thus we suspect that the spatiotemporal pattern of these waves may not be actively controlled, but is merely a byproduct of imperfect synchronization between oscillators. The emergence of travelling waves has been observed in other oscillatory systems with imperfect synchronization (e.g. due to delays), and can be predicted by fairly general models of coupled oscillators (Ermentrout, 2010). These theoretical tools have also been used to understand the spatiotemporal dynamics of *her1* expression, e.g. (Ares et al., 2012; Morelli et al., 2009). Here we revisit some of these arguments, by modifying equation S1 to a more general form that explicitly considers oscillator synchronization. Specifically, we consider a 1D array of cells ($i = 1, 2, \dots, N$, with $i = 1$ anterior and $i = N$ posterior) and describe the phase dynamics by:

$$\frac{\partial \phi_i}{\partial t} = \omega_i + H_i(\phi_{i+1} - \phi_i) + H_i(\phi_{i-1} - \phi_i) \quad (\text{S18})$$

commonly referred to as the Kuramoto model[‡] (Kuramoto 1984). Here, $\omega_i \equiv 2\pi/T_i$ describes the oscillator frequencies, and $H_i(\phi)$ the coupling between oscillators. Following (Ermentrout, 2010), a natural choice for the coupling term is $H_i(\phi) = k_i \sin(\phi + \Phi_i)$, where k_i is the coupling strength and Φ_i the effective coupling delay[§]. Given this equation, we can ask - under what conditions do the oscillators successfully synchronize; or, the complementary question - under what conditions do travelling waves emerge as a result of imperfect synchronization?

Interestingly, we found that many conditions resulted in the formation of travelling waves. As has been hypothesized elsewhere (Giudicelli et al., 2007), a gradient in frequencies along the anterior-posterior (AP) axis, $\omega_i \neq \text{const}$, results in travelling waves along a single direction. However, we also found that if either the coupling strength, k_i , or the coupling phase delay, Φ_i , varied along the AP axis, then this too resulted in travelling waves. Given that there are multiple signaling gradients with the PSM, which could feasibly affect the oscillator frequency, coupling or time delay (Ay et al., 2014), then it is unsurprising that travelling waves will emerge.

Even in the complete absence of spatial gradients (i.e. ω_i, k_i, Φ_i are constant), travelling waves can still form. Consider the case of a ‘cut’ boundary condition at the anterior end $i = 1$ - here, ‘cut’ means that the most anterior cells are coupled only on their posterior side. This could be achieved, for example, if cells in mature somites stopped being coupled to the oscillations in the PSM - either by failing to signal to the PSM, or by terminating *her1* oscillations completely.[¶] Given the assumption of a cut boundary condition, the system is described by:

$$\frac{\partial \phi_1}{\partial t} = \omega + H(\phi_2 - \phi_1) \quad (\text{S19})$$

i.e. the 1st oscillator takes no input from its anterior neighbour. Then, for the remaining oscillators we have:

$$\frac{\partial \phi_2}{\partial t} = \omega + H(\phi_3 - \phi_2) + H(\phi_1 - \phi_2) \quad (\text{S20})$$

etc. Assuming solutions of the form $\phi_i = \Omega t + A_i$, then:

$$\Omega = \omega + H(A) \quad (\text{S21})$$

$$\Omega = \omega + H(A) + H(-A) \quad (\text{S22})$$

etc., which has a stable solution of phase-locked oscillations with overall frequency Ω , and a phase gradient defined by $H(-A) = 0$. For the choice of $H(\phi) = k \sin(\phi + \Phi)$, we have $A = \Phi$ and $\Omega = \omega + k \sin(2\Phi)$. Thus, in the complete absence of spatial gradients, but with a cut anterior boundary condition, we have a linear phase gradient $\phi_i = \Omega t + \Phi i$ i.e. waves that travel from posterior to anterior (provided $\Phi > 0$). We confirm this with simulations, using a cut boundary condition in the anterior and a reflective boundary condition in the posterior.

Taken together, given a set of coupled oscillators operating with phase delays, having spatially varying inputs and unknown boundary conditions, it is not surprising to see travelling waves (consistent with previous work e.g (Ares et al., 2012; Morelli et al., 2009)). Therefore, without any clear spatiotemporal perturbations of the *her1* travelling waves, it is difficult to determine to what extent these travelling waves are functional, or could simply be the result of imperfect synchronization. In particular, as discussed in the main text, the presence of a ≈ 4 -cycle delay between somite size determination and the appearance of morphological boundaries suggests that the *her1* dynamics are likely unimportant in the most anterior region of the PSM.

[‡]We emphasize that our model does not aim to describe all features of the waves (e.g. the anterior increase in oscillator amplitude), but merely to show that a very simple model does quite well in capturing the qualitative wave dynamics.

[§]this is not an explicit time delay, for details see (Ermentrout, 2010)

[¶]Note that previous studies support the notion of somite maturation forming an anterior boundary condition e.g. in ripply morphant embryos (Kawamura et al., 2005), in which somite maturation is impaired, *her1* expression persists more anteriorly.

A small effect of *her1* travelling waves on the Clock and Scaled Gradient Model

In our model, we have assumed that the entire PSM oscillates synchronously (i.e. there is no phase gradient) and found that this could qualitatively explain our data. However, measurements of *her1* dynamics *in vivo* show that there is a phase gradient (i.e. travelling waves) within the PSM (Soroldoni et al., 2014). We therefore wished to ask to what extent such a phase gradient would affect the results of our model.

To do this, we assumed a simple linear phase gradient:

$$\phi(x, t) = \frac{2\pi t}{T} + kx \quad (\text{S23})$$

where k is a constant that controls the magnitude of the gradient (with the sign determining the direction of the travelling waves). We then repeated the wildtype simulations with this modified phase profile, using $|k| = 0.5$, corresponding to an initial phase difference of 10 rad across the PSM). The results are shown in Fig. 7 A and B.

Supplementary References

- Ares, S., Morelli, L. G., Jorg, D. J., Oates, A. C. and Julicher, F.** (2012). Collective modes of coupled phase oscillators with delayed coupling. *Phys Rev Lett* **108**, 204101.
- Ay, A., Holland, J., Sperlea, A., Devakanmalai, G. S., Knierer, S., Sangervasi, S., Stevenson, A. and Ozbudak, E. M.** (2014). Spatial gradients of protein-level time delays set the pace of the traveling segmentation clock waves. *Development* **141**, 4158-67.
- Cotterell, J., Robert-Moreno, A. and Sharpe, J.** (2015). A Local, Self-Organizing Reaction-Diffusion Model Can Explain Somite Patterning in Embryos. *Cell Syst* **1**, 257-69.
- Ermentrout, G. B., Terman, David H.** (2010). *Mathematical foundations of neuroscience*: Springer Science & Business Media.
- Giudicelli, F., Ozbudak, E. M., Wright, G. J. and Lewis, J.** (2007). Setting the tempo in development: an investigation of the zebrafish somite clock mechanism. *PLoS Biol* **5**, e150.
- Hamaratoglu, F., de Lachapelle, A. M., Pyrowolakis, G., Bergmann, S. and Affolter, M.** (2011). Dpp signaling activity requires Pentagone to scale with tissue size in the growing *Drosophila* wing imaginal disc. *PLoS Biol* **9**, e1001182.
- Kawamura, A., Koshida, S., Hijikata, H., Ohbayashi, A., Kondoh, H. and Takada, S.** (2005). Groucho-associated transcriptional repressor ripply1 is required for proper transition from the presomitic mesoderm to somites. *Dev Cell* **9**, 735-44.
- Kuramoto, Y.** (1984). *Chemical Oscillation Waves, and Turbulence*. Mineola, New York: Dover Publications, Inc.
- Lauschke, V. M., Tsiairis, C. D., Francois, P. and Aulehla, A.** (2013). Scaling of embryonic patterning based on phase-gradient encoding. *Nature* **493**, 101-5.
- Morelli, L. G., Ares, S., Herrgen, L., Schroter, C., Julicher, F. and Oates, A. C.** (2009). Delayed coupling theory of vertebrate segmentation. *Hfsp J* **3**, 55-66.
- Soroldoni, D., Jorg, D. J., Morelli, L. G., Richmond, D. L., Schindelin, J., Julicher, F. and Oates, A. C.** (2014). Genetic oscillations. A Doppler effect in embryonic pattern formation. *Science* **345**, 222-5.